Application of Solidification Theory to Rapid Solidification Processing

W. J. Boettinger, J. W. Cahn, S. R. Coriell,
J. R. Manning, and R. J. Schaefer
Metallurgy Division
Center for Materials Science
National Bureau of Standards
Washington, D.C. 20234

Semi-Annual Technical Report
Period Covered: April 1, 1981 to September 30, 1981
ARPA Order No. 3751

Report Issued: February 1982

Prepared for
Defense Advanced Research Projects Agency
Arlington, Virginia 22209

Program Code No: 9D10
Effective Date of Contract: April 1, 1979
Contract Expiration Date: March 31, 1982
Principal Investigator: J. R. Manning
(301) 921-3354

Table of Contents

Application of Solidification Theory to Rapid Solidification Processing

1. Technical Report Summary

This semi-annual technical report for ARPA Order 3751 covers the period April 1, 1981 to September 30, 1981. Significant accomplishments during that period include:

Interface Stability during Rapid Solidification

- Cellular structures, indicating interface instability, were found in several Al-Mn and Al-Ag surface melted alloys which were resolidified at rates as much as 5 to 10 times larger than that theoretically required to produce cell free structures. These results indicate that somewhat larger velocities than expected are needed to produce absolute stability.
- At sufficiently large resolidification velocities (2 cm/s), an absence of cellular structure was found in Al-Mn alloys containing 0.25 wt% Mn. This indicates that plane front growth was established, where rapid solidification stabilizes the solidifying interface, thus tending to avoid lateral alloy segregation.

Extended Solid Solubility

- Achieved single phase partitionless crystallization in Ag-28 wt% Cu, a composition well into the two-phase solid region of the phase diagram, by solidification at velocities above 70 cm/s.

Glass Formation

- Related the observed composition dependence of the critical velocity for glass formation in Pd-Cu-Si alloys to phase diagram features. Related the tendency for crystallite nucleation in the copper-rich composition range to Pd-Cu-Si phase diagram features.

Task Objective

The objective of this work is to develop guidelines based on kinetic and thermodynamic solidification theory for prediction and control of rapid solidification processes. In particular, segregation effects and rules governing the formation of equilibrium and non-equilibrium phases, including metallic glasses, will be investigated. Areas where significant improvements in alloy properties can be produced by rapid solidification will be emphasized.

Technical Problem and General Methodology

Rapid solidification techniques make it possible to produce new types of materials having significantly better properties than conventionally processed materials. However, improved predictive techniques and control of rapid solidification processes are needed. The current studies are focussed on the science underlying areas where improved materials can be obtained in order to provide such prediction and control. This work is both theoretical and experimental.

Three major ways in which rapid solidification technology provides improved materials are:

A. Production of alloys with new compositions, microstructures and phases.

B. Production of more homogeneous alloys.

C. Production of alloys with improved microstructures.

Accomplishments to date in each of these areas will now be described in more detail with mention being made of areas where further testing of rapid solidification theory is needed.

In application A, particular success has been achieved. (1) A directional solidification apparatus was built which allowed direct knowledge of fast solidification velocities. These velocities usually have not really been

known in previous rapid solidification investigations. By rapid quenching of Pd-Cu-Si alloys of varying copper composition, NBS investigators were able to determine maximum solidification velocities for dendrite and eutectic crystallization and,consequently, the conditions for glass formation. A sharp transition from crystalline to amorphous solidification was consistently found when the solidification velocity was increased above about 2-20 mm/s in these alloys, depending on composition. These results then were used to relate glass-forming tendencies to phase diagram features as well as to kinetic models of crystallization based on the diffusional sorting of solute in the liquid. At some compositions and velocities, independent nucleation of crystallites occurred even in the presence of a substrate. Nevertheless, the experimental results generally confirmed the importance of solute redistribution on the maximum crystal growth rate in these alloys. Crystal growth rates rather than nucleation rates were the main factor in determining whether amorphous or crystalline solidification was obtained. (2) Principles which allow prediction of maximum limits on extended solid solubility in rapidly solidified alloys and phase sequences for metastable alloys were established. Experiments are being initiated to test the predicted kinetic and thermodynamic limits on extended solid solubility. Because of kinetic limitations it may in some cases not be possible to obtain the amounts of extended solid solubility that would be thermodynamically allowed. Here again it will be important to establish the rapid solidification velocities that are sufficient to prevent the sorting of constituents into two phase rather than one phase structures.

In application B, it was predicted that, when solidification occurs rapidly enough, the stable shape of the solidification interface is planar rather than dendritic. Then, interdendritic alloy segregation will be avoided and a more nearly homogeneous alloy obtained. Planar interfaces also are stable at very slow velocities. However, at intermediate velocities, nonplanar

(cellular or dendritic) interfaces are produced. Calculations indicate that the high velocity planar regime will occur at practical rapid solidification rates in a number of alloys. Experiments are being performed on Al-Ag alloys to test this prediction. An electron beam melting system has been modified to produce a measurable energy distribution in the beam during surface melting. This melting is followed by refreezing. When this beam is pulsed or scanned across the surface, solidification velocities can be calculated to allow comparison of experimental observations with theory. Current results indicate that transient conditions during the time that the solidification rate is increasing may be important.

In application C, it may be noted that a number of alloys can be expected to exhibit cellular growth and consequent fine scale intercellular segregation even at very high solidification velocities. To investigate this, a quantitative theory of microsegregation has been formulated which shows the influence of cellular spacing, solidification velocity, and the amplitude of the instability at the interface on the magnitude and distribution of the intercellular segregation. Lack of equilibrium in the composition distributions at the solidification interface could significantly affect the parameters that should be used in calculations of this segregation.

A more detailed listing, outlining current accomplishments in these areas of rapid solidification application, is now given.

Summary of Technical Results, Important Findings and Conclusions - Highlights of NBS Accomplishments (April 1979-Sept. 1981)

A. New Compositions, Microstructures and Phases

Extended Solid Solubility

- Theoretically derived rules relating maximum enhanced solid solubility to phase diagram features.

- Applied these rules to silicon alloys and found agreement with results reported in the literature.
- Experimentally achieved enhanced solid solubility from electron beam melting and resolidification in Ag-Cu alloys. These experiments use Ag-Cu as an example of a broad class of alloys with a retrograde solidus, where enhanced solubility must be caused by a solute trapping mechanism.
- Achieved single phase partitionless crystallization in Ag-28 wt% Cu, a compositions well into the two-phase solid region of the phase diagram, by solidification at velocities above 70 cm/s.

Glass Formation

- Developed theory providing boundaries for the region in the phase diagram where partitionless solidification is thermodynamically forbidden. In this region, a two-phase structure must be created if crystallization is to occur.
- Showed that, because diffusion processes are required to sort out the constitutents into two-phase eutectic microstructures in this region, eutectic crystallization velocities typically will not exceed 5 cm/s, making glass formation easy during rapid solidification.
- Experimentally determined maximum crystallization velocity for Pd-Cu-Si two-phase eutectic alloy. The strikingly sharp transition from crystalline microstructure to metallic glass as the solidification rate was accelerated, verified the basic premise that growth rate control rather than nucleation control was the factor preventing crystallization.

- o Measured the sequences of microstructures formed as functions of composition and solidification velocity in Pd-Cu-Si alloys as the solidification velocity was increased and determined the composition dependence of the critical velocity for glass formation. Found nucleation of isolated crystallites to be important on the copper-rich side of the eutectic composition but not on the copper-poor side.
- o Related the observed composition and velocity dependencies, including the nucleation effects on the copper-rich side of the eutectic, to Pd-Cu-Si phase diagram features.

Alloy Phases

- o Calculated thermodynamic bounds on the degree of metastability that can be obtained from rapid solidification.
- o Developed techniques for utilizing equilibrium phase diagrams for estimation of rapid solidification effects.
- o Produced criteria for recognizing when rapid solidification has given a solid alloy that is closer to equilibrium than obtained by conventional solidification.
- o Developed general rules governing the sequences in which combinations of metastable phases can occur in multicomponent alloys.

B. Production of More Homogeneous Alloys

Interface Stability for Production of More Homogeneous Alloys

- o Developed morphological stability theory to include effects that become important at high solidification velocities, including (1) surface tension effects and (2) deviations from local equilibrium at the solidification interface.

- o Showed that, contrary to the trends at slower velocities, plane front solidification becomes increasingly stable with increasing velocity at rapid solidification velocities. This implies that alloy segregation due to interface instability might be completely avoided at very rapid solidification velocities.
- o Cellular structures, indicating interface instability, were found in several Al-Mn and Al-Ag surface melted alloys which were resolidified at rates as much as 5 to 10 times larger than that theoretically required to produce cell free structures. These results indicate that somewhat larger velocities than expected are needed to produce absolute stability.
- o At sufficiently large resolidification velocities (2 cm/s), an absence of cellular structure was found in Al-Mn alloys containing 0.25 wt% Mn. This indicates that plane front growth was established, where rapid solidification stabilizes the solidifying interface, thus tending to avoid lateral alloy segregation.

C. Production of Alloys with Finer Microstructures

Segregation Produced by Unstable Solidification Interfaces

- o Examined directional and anisotropic factors influencing solidification interface stability and showed that, while cells and dendrites formed as a result of interface breakdown will follow crystallographic directions at moderate velocites, they instead will follow temperature gradient directions when velocities are sufficiently high.
- o Calculated as a function of solidification velocity the wavelength (cell-size) at which interface instability occurs.
- o Developed theory relating amount of intercellular segregation to solidification velocity, distribution coefficient and amplitude of interface instability. Calculated typical values for segregation in rapidly solidified alloys.

Plans and Implications for Future Work

For constant velocity solidification, morphological stability theory delineates the temperature gradients required for plane front solidification of a specific alloy. Using electron beams, surface heating of metals has been carried out in the current work with sufficiently well-characterized thermal input to permit reliable use of computer models of melting and solidification. This electron beam work has been directed to the testing of theories developed earlier in this contract in order to provide predictions of circumstances where plane front solidification and resulting improved homogeneity in rapidly solidified alloys can be expected. Our results confirm that planar solidification interfaces can be achieved by rapid solidification. However, it was found that the velocities to produce stability were considerably larger than expected since cellular microstructures persisted even at solidification velocities 5 to 10 times larger than the expected velocity for absolute stability.

Several possible explanations for the persistence of cells at higher solidification velocities than those predicted by absolute stability are now under investigation, including the more detailed analysis of the effect of a velocity-dependent solute distribution coefficient, k, and the effects of trace amounts of low k impurities in the melt zone.

Work has continued on the development of a quantitative theory of micro-segregation (alloy composition as a function of position on a microscopic scale) during alloy solidification. We are developing a numerical algorithm based on a Fourier expansion to calculate the temperature field in the vicinity of a non-planar interface of specified shape. For equal thermal properties in the solid and liquid, an alternative method developed by R. F. Sekerka will be used to provide a test of the Fourier method. The eventual goal is to self-consistently calculate interface shapes and solute segregation during rapid solidification.

The importance of both growth kinetics and phase diagram features in the development of microstructure and extended solid solubility in rapidly solidified alloys is being investigated. Thermodynamic limits are provided by special phase diagram features, such as the T_0 curve which is the locus of compositions and temperatures where the liquid and crystalline solid free energies have the same value. T_0 represents the highest interface temperature at which the partition coefficient can be unity. Generally, further kinetic cooling should be required for partitionless solidification, which can produce extended solid solubility. If a molten alloy with composition in a normally two-phase regime is cooled below T_0 so rapidly that separation into segregated phases kinetically cannot occur, crystalline alloys exhibiting greatly enhanced solid solubility can be produced. It is planned to investigate such situations further in alloys such as Ag-Cu, where the T_0 curve lies only 100 °C or so below the melting point.

On the other hand, when the T_0 curve falls rapidly to extremely low temperatures, the limit of the partition coefficient even at high velocities cannot approach unity for compositions near the middle of the two-phase region. Then, if the alloy is cooled so rapidly that separation into two crystalline phases is not possible, a metallic glass can be formed. Experiments done on this contract on the composition and solidification velocity dependence of the microstructural forms and nucleation processes in Pd-Cu-Si alloys show strong correlations with phase diagrams features, which are still being analyzed.

Since extended solid solubility in crystalline alloys and conditions for formation of metallic glass are limited by kinetic as well as thermodynamic considerations, growth kinetic limitations necessarily will continue to be an important part of the present research. It is these kinetic considerations

that determine how fast the solidification process must be in order to produce significant rapid solidification effects.

2. Report of Technical Progress and Results

Electron Beam Surface Melting Studies of Interface Stability during Rapid Solidification

When a material solidifies under conditions of morphological stability, the resulting solid will be homogeneous in composition on a microscopic scale, whereas instability will result in the formation of a solid containing a cellular pattern of solute segregation. At conventional solidification velocities, stability is favored by steep positive temperature gradients and low solidification velocities. However, morphological stability theory predicts that when an alloy solidifies at a sufficiently rapid velocity into a liquid with a positive temperature gradient, capillarity effects will stabilize plane front solidification at concentrations much greater than those predicted in the absence of capillarity, thus eliminating cellular microsegregation. At sufficiently large velocities, the maximum alloy concentration at which this stable plane-front solidification occurs is given by the absolute stability criterion, namely

$$C_{\infty a} = k^2 T_M \Gamma V / [m(k-1)D]$$

where k is the solute distribution coefficient, T_M is the equilibrium melting point, Γ is the surface energy parameter, V is the solidification velocity, m is the liquidus slope, and D is the solute distribution coefficient. When considering the solidification of aluminum alloys, it is thus predicted that a solute having a low value of k (such as iron, for which $k \tilde{\sim} 0.03$) can be present only at very low concentrations if the absolute stability criterion is to be satisfied at solidification velocities of 10^{-2} to 10^{-1} m/s. In contrast absolute stability can be expected at these velocities in the presence of

solutes such as silver (k = 0.41) or manganese (k = 0.79) at concentrations of 0.1 to 1 weight percent. The stabilization of plane-front solidification at high velocities has been seen by workers using laser pulses a few nanoseconds in duration to melt the surface of doped silicon crystals. In this case the solidification velocities are typically a few meters per second but the melt depths are necessarily extremely small. At these velocities there is good evidence that the solute distribution coefficient, k, depends on the solidification velocity and becomes closer to unity than its equilibrium value. In metals, we are generally interested in deeper melts, where the solidification velocities cannot be so high. Thus, it is more significant to observe absolute stability at 10^{-2} to 10^{-1} m/s, at which velocities k may not be expected to deviate greatly from its equilibrium value.

Following surface melting of an alloy by a directed energy source such as an electron beam or a laser, the solid-liquid interface during resolidification will experience a sequence of velocities and temperature gradients. If during this sequence the interface at no time encounters conditions under which it is morphologically unstable, then one can expect the alloy to solidify without any cellular microstructure. If the interface encounters even briefly conditions under which it is morphologically unstable, it may develop a cellular structure. The conditions required for reversion of a cellular microstructure to plane front solidification are not known and are not necessarily closely related to the conditions for morphological stability of a planar interface. Thus the most certain way to avoid cellular substructures is to use a melt sequence which never subjects the solid-liquid interface to conditions of morphological instability.

If a surface melt is carried out under conditions which lead to one-dimensional heat flow (heating over a large area for a short time), most of the resolidification takes place at an almost constant velocity after an initial transient during which the velocity accelerates from zero at the bottom of the melt. A substantial positive gradient is present in the liquid during the transient phase, but it drops to almost zero during the constant velocity solidification. The heat flow calculations indicate that for the Al-Ag and Al-Mn alloys considered here, if the velocity during the constant velocity solidification is large enough to produce absolute stability, then the gradients during the transient phase are large enough to produce stability while the interface is accelerating. Thus, unstable conditions can be totally avoided. For two or three-dimensional heat flow, no such simple relationship exists and the sequence of solidification conditions must be considered in more detail to determine if a region of instability is entered.

Electron beam melting experiments with Al-Ag and Al-Mn have been carried out using pulsed or scanned circular spots. Detailed studies of the magnitude and distribution of the energy in the electron beam were used to give the best possible correlation of the melting parameters to those assumed in the heat flow models.

The general conclusion of the surface melting experiments has been that cellular microstructures were present at solidification velocities considerably larger than those predicted to be required for absolute stability. However, in a series of Al-Mn alloys which were electron-beam melted under conditions which should produce resolidification at approximately 2×10^{-2} m/s, it was found that a cellular structure was present in the electron beam melt zone at 1 wt% Mn but not at 0.25 wt% Mn. In both alloys, a cellular structure was present in the chill-cast substrate. The absence of the cellular structure in the 0.25% Mn alloy is interpreted as a manifestation of absolute stability,

but it appeared only at a solidification velocity 5-10 times as large as predicted by the absolute stability equation given above. Similarly, in Al-Ag, cells were seen at velocities greater than those predicted for absolute stability.

A paper, entitled "Morphological Stability of Electron Beam Melted Aluminum Alloys," by R. J. Schaefer, S. R. Coriell, R. Mehrabian, C. Fenimore, and F. S. Biancaniello, was presented at the November 1981 Meeting of the Materials Research Society in Boston, and has been submitted for publication in the proceedings of that meeting. This paper which is included in the appendix (pp. 16-25) to the present report describes in more detail the work discussed above.

Extended Solid Solubility

Experiments have been performed on rapid solidification of Ag-Cu alloys to produce enhanced solid solubility. This sytem is a simple eutectic phase diagram between the Cu-rich and Ag-rich terminal phases. The maximum solubility of copper in silver is about 8.8 wt%. Both terminal phases are face-centered cubic and the T_0 curve is expected to be only 100 °C or so below the alloy liquidus curves. Thus, this alloy provided a particularly favorable condition for producing extended solid solubility by partitionless solidification. Kinetically, the important question is at what solidification velocity does the microstructure change from a two-phase eutectic or dendrite plus eutectic microstructure to a single phase supersaturated solution with the same composition as the liquid.

Experiments have been performed on Ag-15 wt% Cu and Ag-28 wt% Cu (compositions normally consisting of two solid phases) using electron beam surface melting and melt spinning. Melt spun samples show microstructures consisting of single phase columnar grains oriented perpendicular to the chill surface of the ribbon. TEM examination of these alloys show them to be single phase.

These compositions when solidified at slower velocities produce two-phase structures with a solubility limit of Cu in Ag of about 8.8 wt%. Thus, a considerable amount of extended solid solubility has been produced.

One difficulty with melt spinning is that the growth rate is difficult to estimate and only a limited range of growth rates are obtained. Because of this limitation, we have employed electron beam melting in a geometry similar to a weld pass. By varying the scan speed, solidification velocities from $\sim$ 1 cm/s to 70 cm/s have been achieved. At 70 cm/s the Ag-28 wt% Cu alloy is single phase. At speeds below 36 cm/s the alloy consists of bands of high and low copper content with a spacing of approximately 1 μm. These bands are generated parallel to the solid-liquid interface. This microstructure appears to occur at intermediate velocities between that which produces dendritic or eutectic structure and that which produces single phase growth of a uniform composition. The mechanisms for this banding are currently under investigation.

Metallic Glass Formation

A large range of compositions about many eutectics, especially those involving line compounds, must crystallize from the liquid as multiphase solids even if that crystallization is far from equilibrium. This range lies between the T_0 curves of the phases in the eutectic. In this range, massive (partitionless) crystallization is forbidden, and the maximum crystallization rate will depend on the details of the diffusive sorting of the components in the liquid into the crystalline phases and the creation of crystal-crystal interfaces.

In experiments on Pd-Cu-Si alloys, the maximum crystallization rate was determined as a function of Cu composition with slightly varying Si composition lying along a line in the ternary system. This maximum rate was determined by observing the changes in microstructure as solidification velocity was increased.

A number of results related to this study are described in detail in the appendix (pp. 27-30), "The Effect of Alloy Constitution and Crystallization Kinetics on the Formation of Metallic Glass." Several pertinent results are that (1) glass formation tends to be easiest at compositions intermediate between the limiting equilibrium phases but not necessarily exactly at the eutectic composition, (2) on the Pd-rich side of the eutectic the transition from dendritic growth to eutectic growth with increasing growth rate determines the critical conditions for avoidance of crystallization and (3) on the Cu-rich side of the eutectic the formation of completely glassy structures is prevented by the nucleation of isolated crystallites of a cubic copper-rich phase directly from the melt. STEM analysis shows the interdendritic regions to be amorphous and to have compositions closer to the easy glass-forming composition than the average alloy composition.

Metallic glass formation provides an example of the importance of growth kinetics in the development of microstructure in rapidly solidified alloys. Production of extended solid solubility by partitionless crystallization is another situation where kinetic limits are important. This general question is discussed in a paper, entitled "Growth Kinetic Limitations During Rapid Solidification" by W. J. Boettinger, presented at the November 1981 Meeting of the Materials Research Society in Boston, and submitted for publication in the proceedings of that meeting. The paper is included in the appendix (pp. 31-47) to the present report.

TO BE PUBLISHED, Rapidly Solidifed Amorphous & Crystalline Alloys, ed. by B. H. Kear and B. C. Giessen, Elsevier North Holland, New York 1982.

MORPHOLOGICAL STABILITY OF ELECTRON BEAM MELTED ALUMINUM ALLOYS

R. J. SCHAEFER, S. R. CORIELL, R. MEHRABIAN, C. FENIMORE, AND F. S. BIANCANIELLO
National Bureau of Standards, Washington, D.C. 20234

ABSTRACT

For constant velocity solidification, morphological stability theory delineates the temperature gradients required for plane front solidification of a specific alloy. Using electron beams, surface heating of metals can be carried out with sufficiently well characterized thermal input to permit reliable use of computer models of melting and solidification. From numerical calculations, the growth velocity and temperature gradients as a function of position during resolidification can be obtained; combining these results with (constant velocity) morphological stability theory indicates the resolidification regimes for which the plane front is unstable. Presumably, completely planar solidification may be attained by selecting heating modes such that the region of instability is totally avoided, but the expected interface morphology is more difficult to predict if the interface passes briefly through an unstable region and then re-enters a region of stability. Aluminum-silver and aluminum-manganese alloys were melted under an electron beam with particular emphasis on attaining solidification sufficiently rapidly to satisfy the gradient-independent absolute stability condition. It was found that the velocities required to produce stability were considerably larger than expected.

INTRODUCTION

Under the conditions normally encountered in conventional crystal growth techniques such as the Bridgman or Czochralski process, the theory of constitutional supercooling [1] gives good guidelines for the temperature gradients and growth velocities which are required for plane-front solidification of a dilute alloy. It predicts that steep gradients and slow growth velocities are required to prevent the formation of a destabilizing layer of supercooled liquid ahead of the planar interface. Morphological stability theory [2] is based on an analysis of the actual process by which a planar interface can transform to a non-planar one, and for the conventional crystal growth processes its predictions do not vary greatly from those of the constitutional supercooling theory. However, the theory of morphological stability can account for the effects of phenomena such as surface energy and interfacial kinetics, which under more severe crystal growth conditions can dominate over temperature gradient effects. The research described here is directed toward an understanding of the stability of planar solid/liquid interfaces which solidify at high velocities (above about 10^{-2}m/s): for such growth rates morphological stability theory shows that an absolute stability regime exists in which plane-front solidification is stabilized by increasing growth velocity and is insensitive to temperature gradients.

When velocities become very high, solute trapping is expected to occur, leading to a velocity-dependent distribution coefficient which is closer to

unity than is the equilibrium coefficient. While this effect is expected to provide additional stabilization for rapidly moving interfaces, its influence on morphological stability has not been analyzed in detail, and there is little quantitative information on the kinetics of trapping in metallic systems.

Solidification at the velocities required to attain absolute stability can be achieved by several methods, but with most of them it is difficult to characterize the conditions under which the solidification occurs. For this study an electron beam has been used to provide energy at high density to metal surfaces and heat flow theory has been used to compute the resulting surface melting and solidification behavior. It was therefore not necessary to estimate reflectivities or heat transfer coefficients.

THEORY

Morphological Stability. The application of morphological stability theory to rapid solidification was described previously [3,4], with calculations presented for silicon alloys and the Al-Cu system.

Figure 1 shows the form of the predicted stability relationships for aluminum-silver alloys on a plot of silver concentration in the liquid far from the interface, C_∞, vs the steady state solidification velocity, V. The properties used for these calculations are shown in Table I. The straight lines on the left show the constitutional supercooling relationship

$$C_{\infty cs} = \frac{DkG_L}{m(k-1)V} \tag{1}$$

for four different values of the gradient G_L in the liquid. Here D is the diffusion coefficient of the solute in the liquid, k is the equilibrium distribution coefficient, m is the liquidus slope, and V is the growth velocity. The upward sloping line on the right represents the absolute stability criterion

$$C_{\infty a} = \frac{k^2 T_m \Gamma V}{m(k-1)D} \tag{2}$$

of Mullins and Sekerka [2], where T_m is the melting point of the planar interface without solute and Γ is the ratio of the solid-liquid surface energy to the latent heat of fusion per unit volume. The curved lines are given by morphological stability theory; below the curves plane-front solidification is stable and above them it is unstable. The curves lie close to the straight lines at very small or very large velocities, but the minimum of the curves lies above the intersection of the straight lines. Even in the absence of solid-liquid surface energy, morphological stability theory predicts a minimum concentration at which a cellular structure is expected, i.e., alloys with concentrations less than

$$C_{min} = \{DkL_v/[m(k-1)(k_s+k_L)]\} \tag{3}$$

are always stable, where k_L and k_s are the thermal conductivities of the liquid and solid, respectively. In the case of the Si alloy calculation reported in Ref. [3], C_{min} lies above the intersection of the constitutional supercooling and absolute stability lines, and the minimum of the morphological stability curve here lies just slightly above C_{min}. In contrast, the

TABLE I
Properties Used for Stability Calculations in Al-Ag

Property	Symbol	Value
Diffusion rate in liquid	D	$4.5 \times 10^{-9} m^2/s$
Solute distribution coefficient	k	0.41
Liquidus slope	m	-1.7 K/wt.%
Surface energy parameter	$T_M\Gamma$	1.0×10^{-7} m·K
Latent heat of fusion	L	$1.08 \times 10^9 J/m^3$
Thermal conductivity of liquid	k_L	90.4 J/s·m·K
Thermal conductivity of solid	k_s	211 J/s·m·K
Thermal diffusivity of liquid	α_L	$3.5 \times 10^{-5} m^2/s$
Thermal diffusivity of solid	α_s	$6.8 \times 10^{-5} m^2/s$

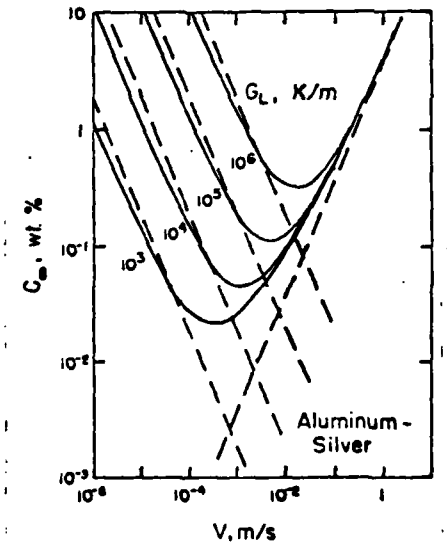

Fig. 1. Stability of Al-Ag alloys for four different values of the of the temperature gradient G_L in the liquid.

calculated value of C_{min} in the Al-Ag system is 6.6×10^{-3} wt. % Ag, which lies below the intersection of all of the absolute stability and constitutional supercooling lines in Fig. 1, except in the case of $G_L = 10^3$K/m. The minimum of the morphological stability curve under these circumstances is

found to lie above the intersection point by a factor of approximately 5. A similar factor can be seen in the computed curves for Al-Cu alloys [4].

To estimate the relative destabilizing influence of different solutes in a given solvent, we can note that in Equations (1) and (2) only the parameters m and k will depend strongly on the solute. The intersection point of these lines occurs at

$$V^* = D(G_L/T_m\Gamma k)^{\frac{1}{2}} \tag{4}$$

and

$$C^* = [(G_L T_m \Gamma)^{\frac{1}{2}}/m][k^{3/2}/(k-1)] \tag{5}$$

A plot of $mC^*/(G_L T_m \Gamma)^{\frac{1}{2}}$ vs $(V^*/D)(T_m\Gamma/G_L)^{\frac{1}{2}}$ (Fig. 2) thus illustrates the approximate relative effect of solutes with different k values. Particularly significant is the strong destabilizing effect of solutes having very low k values. It is evident from Figure 2 that plane-front solidification in the absolute stability regime will be difficult to attain for solutes having low k if local equilibrium holds at the solid-liquid interface.

Pulsed laser annealing experiments [5] have demonstrated that at high solidification rates stable plane-front solidification can, as expected, occur at concentrations far greater than those predicted by constitutional supercooling. However, in several silicon alloy systems which exhibit retrograde solidus curves, high speed plane-front solidification can occur at concentrations much greater than that of the maximum equilibrium solid solubility, thus indicating that solute trapping is taking place.

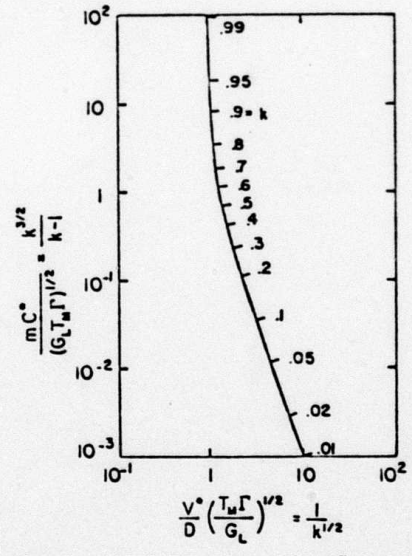

Fig. 2. Normalized composition and velocity at the intersection of the constitutional supercooling and absolute stability lines. The minimum of the morphological stability curve lies somewhat above this intersection.

For an attempt to quantify morphological stability effects at high solidification velocities in aluminum alloys, it is thus advantageous to select an alloying addition having a large k value. Ruling out elements with high vapor pressure such as zinc, which might be lost during surface melting, we find silver, with k = 0.41, as a useful alloying addition. For manganese k = 0.79 [6] and stability should be quite easy to attain.

Surface Melting. The solidification velocities required to enter the region of absolute stability cannot be attained by steady-state unidirectional solidification, which is the condition assumed in generating curves such as those in Figure 1 from morphological stability theory. When rapid solidification is produced by surface melting, by either a pulsed or a scanned heat source, the interface experiences a sequence of gradient and velocity conditions. The melted region can be expected to be free of cellular substructure only if the interface at no stage of this sequence enters a region of morphological instability. Once a cellular interface has formed, the conditions required (such as a change of solidification velocity) to cause it to revert to a planar interface are not known, i.e., the prediction that plane-front solidification is stable does not imply that an established cellular interface is unstable.

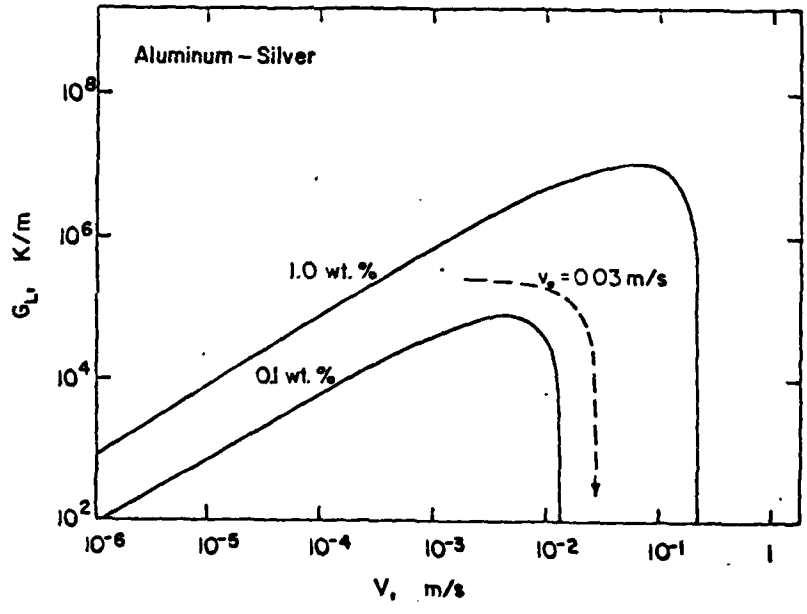

Fig. 3. Alternate representation of the stability of Al-Ag alloys. The unstable region lies below the curves. The dashed lines show the trajectories of the G_L and v values experienced by a solid-liquid interface following surface melting by 20 ms long beat pulses with power densities 1.5×10^8 and $2.0 \times 10^8 W/m^2$.

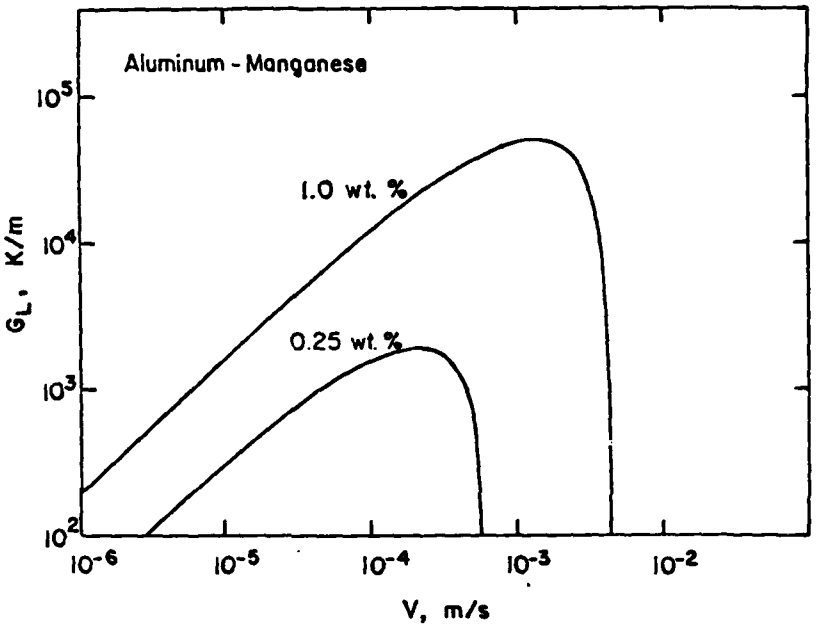

Fig. 4. The stability conditions for aluminum-manganese alloys. Note the low velocities and gradients predicted to produce stable plane-front solidification.

To evaluate the stability of a solid-liquid interface during a surface melting sequence, it is more useful to consider an alternate representation of the curves in Figure 1 in which we plot the temperature gradient required to produce stability as a function of velocity for a fixed composition (Figures 3 and 4).

On such a representation we can plot trajectories which represent the sequence of conditions experienced by a solid-liquid interface during a surface melting episode.

In this type of plot, the region of instability lies under the plotted curves and the region of absolute stability lies to the right where, for velocities greater than a critical value, planar interfaces are predicted to be stable for all positive values of G_L. The theoretical curves are still based on the assumption of steady-state solidification conditions. Thus when plotting the time-dependent trajectory of a surface melting experiment on such a graph, there still exists the discrepancy that in the experiment the solute concentrations and gradients at the solid-liquid interface do not have steady-state values. The degree to which the concentration transients might affect the development of interfacial instabilities is not known.

Melting and solidification cycles are based upon heat flow calculations [7,8,9,10]. For the case of one-dimensional heat flow, previous calculations [7] and a numerical code based on the alternating phase truncation method [10] give results in good agreement. Figure 5 shows the melt depth in aluminum as a function of time following 20 millisecond pulses at power densities of

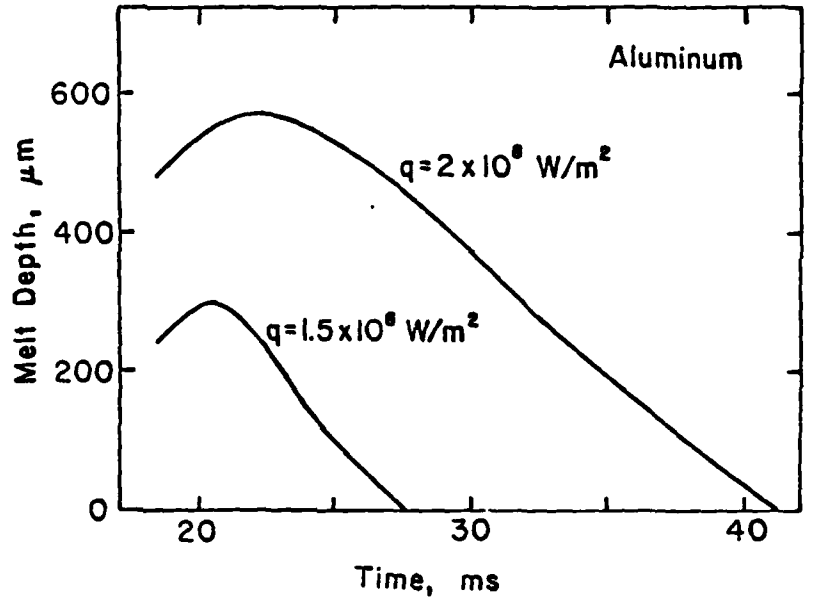

Fig. 5. Interface motion following surface heating of aluminum, as predicted for one-dimensional heat flow by the alternating phase truncation method.

1.5×10^6 W/m^2 and 2×10^6 W/m^2. Note that most of the solidification takes place at an almost constant velocity V_o; during this part of the cycle the temperature gradient in the liquid has dropped to a very low value compared to that in the solid, and the gradient G_s in the solid adjacent to the interface varies by about a factor of 2. Assuming constant G_s we can write $G_L = (L/k_L)(V_o - V)$ for the gradient in the liquid, where V_o is the final almost constant velocity attained by the interface. In Figure 3 the dashed curve represents these G_L values for $V_o = 0.03$ m/s, corresponding approximately to the upper curve in Figure 5. The predicted zone of instability for the 0.1 percent alloy is bypassed.

For heat flow in more than one dimension [8,9], the interface velocities during resolidification are not as constant as they are in the one-dimensional case. For a pulsed stationary spot, the critical parameter is q_a, were q is the absorbed heat flux and a is the radius of the spot. With a sufficiently large value of q_a and small value of the pulse time t, the heat flow is essentially one-dimensional, but at smaller values of q_a or longer pulse times the three-dimensional effects become important. In such cases, the solidification velocity increases steadily as the interface approaches the surface [8].

In the case of melting by a moving circular spot, it is appropriate to consider the trajectory followed by the normal to the solid/liquid interface as the melt zone passes a region on the metal surface (Fig. 6). Considering the process along the central plane of the moving melt zone, the solidification velocity is zero at the deepest point of the melt pool and accelerates to its maximum value as the solid-liquid interface approaches the free surface at the

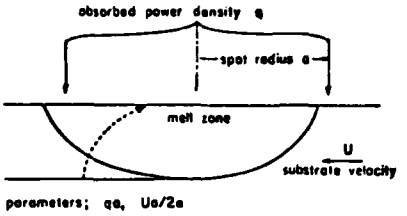

Fig. 6. Schematic representation of the melt pool resulting from scanning an electron beam with a radius a across the surface of a metal at velocity U. The dashed line represents the trajectory followed by the normal to the solid-liquid interface during solidification.

trailing edge of the pool. The local interface velocity is always less than the scanning speed by a factor equal to the cosine of the angle between the scanning direction and the normal to the solid/liquid interface. For this process it was shown in Ref. [9] that the important parameters are qa and $Ua/2\alpha$, where U is the scanning speed. At low (< 1) values of $Ua/2\alpha$, a substantial gradient is present in the liquid at the solid-liquid interface at all times. Thus, as a solid/liquid interface accelerates from zero velocity at the bottom of the melt pool to its maximum velocity at the trailing edge, the ratio G_L/V decreases from infinity to a minimum value which depends on both qa and $Ua/2\alpha$, as shown in Fig. 15 of Ref. [9]. The minimum values of G_L/V as shown in this figure for qa = 3×10^5 W/m and 6.4×10^5 W/m and $Ua/2\alpha$ = 0.45 and 0.75 are much too small to keep the solid-liquid interface above the upward-sloping portions of the curves in Figures 3 and 4. Thus unless V is well above the velocity required for absolute stability the interface can be expected to enter, at least temporarily, the region of instability lying under the curves of Figures 3 and 4.

EXPERIMENT

Surface melting was carried out by means of electron beam heating, using an accelerating potential of 25 kV. Although the absorptivity of metal surfaces for electron beams is not as sensitive to surface preparation as it is for laser beams, it does depend on the accelerating voltage and on the atomic number of the metal target [11]. For the 25 kV beam incident on a flat aluminum target one measures a current entering the sample which is about 14 percent less than the total beam current. However, by measuring the temperature rise of a small thermally isolated aluminum target it is found that the absorbed energy is 7 percent larger than the product of the accelerating voltage and the absorbed beam current. Thus even the backscattered electrons transfer a large fraction of their energy to the sample surface. These factors are taken into account when making calculations based on the thermal input to the sample surface.

If the beam current incident upon an area of the target exceeds a critical density, a plasma is formed and the current entering the sample decreases by approximately 20 percent. This condition must be avoided if a precise knowledge of the magnitude and distribution of the thermal energy input is desired.

To determine the spatial distribution of energy in the electron beam, a method was developed which displays an image of the beam profile on an oscilloscope screen. The electron beam is rastered over a pinhole in a refractory metal sheet and the electrons passing through the pinhole are collected by a Faraday cup. The current collected by this cup controls the intensity of the signal on an oscilloscope screen, which is rastered synchronously with the electron beam deflection. With such a method it was found that if the beam focus current is less than that which produces the sharpest focus, a rela-

tively flat-topped circular beam, with a narrow ring of somewhat higher intensity around the perimeter, is produced. The beam under this condition forms a good approximation to the uniform circular beam assumed in heat flow analyses [8,9].

Surface melts were made on aluminum samples containing 0.1, 0.3, and 1.0 wt. % silver, and 0.1, 0.25, and 1.0 wt. % manganese. Melts were made in a pulsed "spot mode" in which a stationary beam 1 or 2 mm in diameter is directed at a fixed spot on the surface for a period of 20 to 200 ms, and in a "line mode" in which a beam is scanned in a linear track across the sample surface at a velocity, typically, of 10^{-2} to 1 m/s. Microstructures were observed on polished and etched sections by optical and scanning electron microscopy.

Cellular structures were observed with patterns which were sometimes approximately hexagonal, sometimes lamellar, and sometimes irregular. Differing patterns in adjacent grains revealed at least a modest influence of crystallographic anisotropy (Figure 7).

Cellular structures were generally seen at solidification velocities considerably higher than those predicted by the absolute stability criterion. However, the transition to absolute stability was seen in Al-Mn samples which were subjected to 100 ms long pulses with $qa \approx 2 \times 10^5 W/m$ ($a = 10^{-3}m$). In these samples, the 1.0 percent Mn alloy showed a cellular substructure in both the substrate and the electron beam melt zones, the 0.25 percent alloy showed the cellular substructure in the substrate but not in the melt zone, and the 0.1 percent alloy showed no cellular substructure anywhere. These alloys are predicted to show absolute stability at velocities greater than $7 \times 10^{-3}m/s$, $1.8 \times 10^{-3}m/s$, and $7 \times 10^{-4}m/s$, respectively. The rate of solidification under these conditions can be seen from Fig. 9 of Ref. [8] to be greater than $2 \times 10^{-2}m/s$ after the initial transient which accounts for less than 5 percent of the depth of the melt. Thus the velocities required to produce absolute stability were several times as large as those predicted. Cellular substructures were observed in all of Al-Ag alloys (1.0 wt. %, 0.3 wt. %, and 0.1 wt. %), which had predicted velocities of $6 \times 10^{-2}m/s$, $1.8 \times 10^{-2}m/s$, and $6 \times 10^{-3}m/s$, respectively, for absolute stability. In this case only the 0.1 percent Ag alloy was expected to show absolute stability.

DISCUSSION

The solidification velocities required to enter the absolute stability regime in Al-Ag and Al-Mn have been found to be considerably larger than expected on the basis of morphological stability theory calculations which use the equilibrium value of the solute distribution coefficient. Non-equilibrium partitioning of solute, which has been demonstrated in silicon alloys solidified at higher velocities than those used here, normally causes k to approach unity and thus increases the stability of planar interfaces. Although it is in principle possible [3] for the distribution coefficient to deviate from its equilibrium value away from unity over a range of interface velocities, this is regarded as an unlikely explanation for the present observation.

The values of the parameters D and Γ, which appear in the expression for absolute stability, have not been accurately established but the values used in the calculations are unlikely to be in error by a factor larger than 2, which would possibly account for the behavior of the Al-Mn alloys but is insufficient to explain the presence of cells in virtually all of the Al-Ag alloy melts including samples which should have solidified with interface velocities greater than $10^{-1}m/s$.

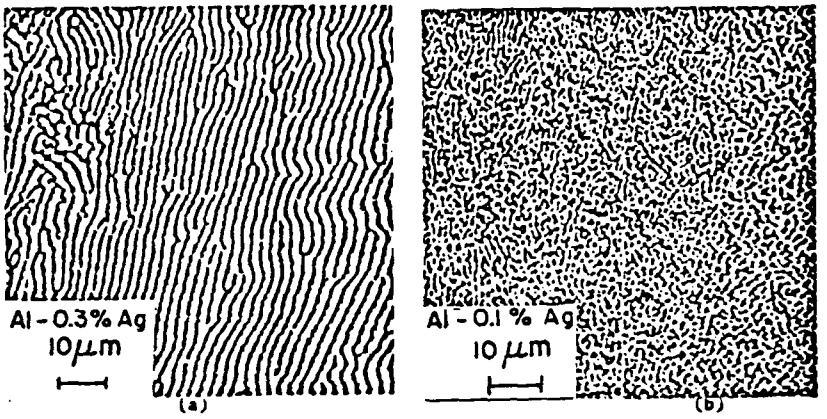

Fig. 7. (a) Lamellar cellular structure in electron beam melted Al-Ag. (b) Irregular cellular structure in electron beam melted Al-Ag.

The possibility that the interface is destabilized by the presence of trace amounts of an impurity having a very low k value would at first seem to be ruled out by the results of an additional experiment in which no cellular substructure was observed in electron beam melts of the 5-9's aluminum stock material from which the Al-Ag alloys were made, but it is not clear that any cellular substructure present in such a material due to the presence of a few parts per million of an impurity such as iron would be detectable on a polished and etched surface. As can be deduced from Fig. 2, the concentration of an impurity such as iron, for which $k \approx 0.03$, which is required to produce instability is extremely small. Such small concentrations of impurities, even if not present in the starting materials, could be introduced during the alloying process, or they could be present as abrasive particles embedded in the sample surface during preparation for melting. Because it is impractical to establish the concentration of impurities at very low levels within the small melt zones, additional experiments are planned in which extra care is directed toward preparing samples in which the possibilities for surface contamination are minimized.

ACKNOWLEDGMENTS

The authors thank W. J. Boettinger and R. F. Sekerka for useful discussions and C. H. Brady and D. B. Ballard for microscopy. This work was supported by DARPA under ARPA Order Nos. 3751 and 4275. Technical Monitor of these contracts is Lt. Col. L. A. Jacobson.

REFERENCES

[1] W. A. Tiller, K. A. Jackson, J. W. Rutter, and B. Chalmers, Acta Met. 1, 428 (1953).

[2] W. W. Mullins and R. F. Sekerka, J. Appl. Phys. 35, 444 (1964).

[3] J. W. Cahn, S. R. Coriell, and W. J. Boettinger, p. 89 in Laser and Electron Beam Processing of Materials, C. W. White and P. S. Peercy, Eds. Academic Press, New York (1980).

[4] S. R. Coriell and R. F. Sekerka, in Rapid Solidification Principles and Technologies II, R. Mehrabian, B. H. Kear, and M. Cohen, Eds., Claitors, Baton Rouge, LA. (1980), p. 35.

[5] C. W. White, S. R. Wilson, B. R. Appleton, F. W. Young, Jr., and J. Narayan, p. 111, Ibid.

[6] T. Takahashi, A. Kamio, and Nguyen An Trang, J. Crystal Growth 24/25, 477 (1974).

[7] S. C. Hsu, C. Chakravarty, and R. Mehrabian, Met. Trans. 9B, 221 (1978).

[8] S. C. Hsu, S. Kou, and R. Mehrabian, Met. Trans. 11B, 29 (1980).

[9] S. Kou, S. C. Hsu, and R. Mehrabian, Met. Trans. 12B, 33 (1981).

[10] J. C. W. Rogers, A. E. Berger, and M. Ciment, SIAM J. Numer. Analysis 16, 563 (1979).

[11] M. von Allmen, p. 6, in Laser and Electron Beam Processing of Materials, C. W. White and P. S. Peercy, Eds., Academic Press, New York (1980).

THE EFFECT OF ALLOY CONSTITUTION AND CRYSTALLIZATION KINETICS ON THE FORMATION OF METALLIC GLASS

William J. Boettinger

Metallurgy Division, National Bureau of Standards, Washington, D.C. 20234

INTRODUCTION

A large range of compositions about many eutectics, especially those involving line compounds, must crystallize from the liquid as multiphase solids even if that crystallization is far from equilibrium. This range lies between the T_o curves of the phases in the eutectic. In this range, massive (partitionless) crystallization is forbidden, and the maximum crystallization rate will depend on the details of the diffusive sorting of the components in the liquid into the crystalline phases and the creation of crystal-crystal interfaces. In particular the maximum eutectic growth rate seems closely related to the minimum cooling rate requirements to form metallic glass for compositions near eutectics (1).

The present paper describes the microstructure of a range of compositions of a model glass former as a function of growth rate up to the critical velocity for glass formation. The results show that, in some cases, the transition from dendritic growth to eutectic growth with increasing growth rate for compositions away from the eutectic determines the critical conditions for the avoidance of crystallization. Fig. 1 shows schematically the *growth* behavior that was anticipated between T_o curves for a simple eutectic system: the maximum eutectic growth rate (dashed line), which is not strongly composition dependent; and the upper velocity bound (solid lines) on the transition from dendritic growth to eutectic growth*. Completely glassy structures will form when the required growth rate due to heat extraction exceeds the maximum eutectic growth rate and dendritic growth is not possible. The relative positions of the three curves can lead to an expanded or a shifted composition range about a eutectic for easy glass forming and the possibility of microstructures consisting of dendrites with interdendritic glass. Such analysis should replace the maximum reduced glass temperature criterion for the detailed location of glass forming composition ranges within a given alloy.

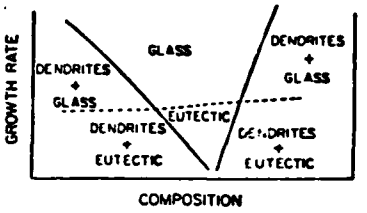

Fig. 1. Maximum crystallization rates for alloys between T_o curves for a simple eutectic system.

EXPERIMENTAL

The glass forming alloy $Pd_{77}Cu_6Si_{17}$ completes crystallization at intermediate cooling rates into a eutectic consisting of two phases γ and ε with compositions determined by microprobe near $Pd_{81}Cu_1Si_{18}$ and $Pd_{73}Cu_{15}Si_{12}$ respectively (1). The γ phase is the ternary modification of Pd_9Si_2. Alloys (Fig. 2b) lying roughly on a line between these two phases were investigated using rapid directional quenching. Thin alloy-filled quartz tubes (0.75 mm ID x 1.5

* An increasing range of composition for eutectic growth with increasing growth rate (or undercooling) exists for many alloys (2-4) and should properly be described by a theory for the morphological stability of eutectic growth.

mm OD x 10 cm long) are quenched in the axial direction from a furnace at 1100 °C into liquid Ga in two stages: first at a relatively slow speed (0.25 mm/s) to establish a crystalline substrate; and second at various constant speeds up to 50 mm/s. This two step procedure eliminates bulk undercooling of the sample, a condition which leads to unknown growth rates unless the nucleation temperature is measured. In the present experiments, microstructures are aligned in the axial direction, indicating directional heat flow, up to quenching speeds of 50 mm/s. At a quenching rate of 2.5 mm/s the measured temperature gradient in the alloy near 700 °C was 500 °C/cm. Two types of microstructural information are obtained from longitudinal sections of the quenched rods: a) the transition of microstructure which exists during the initial acceleration of the isotherms after the speed change; and b) the microstructure at steady state which exists over the major portion of the rod, where the isotherm velocity should nearly approach the quenching speed. Both have been used to construct Fig. 2a, but data points are for steady state results.

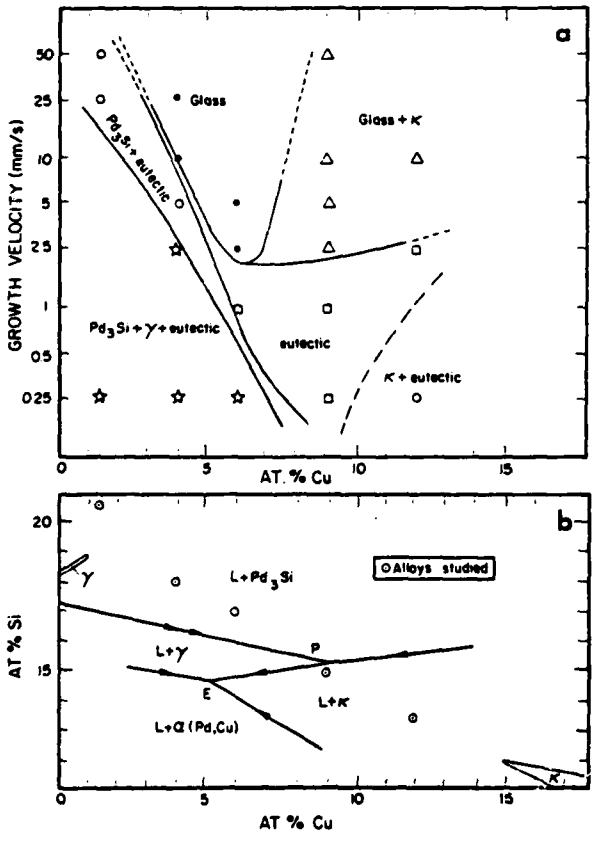

Fig. 2. a) Summary of microstructures obtained and b) liquidus surface with compositions studied.

RESULTS

At slow growth rates, alloys with ≤ 6 at.% Cu form dendrites of Pd_3Si at the highest temperature followed by facetted dendrites of γ directly from the melt (Fig. 3a). At these speeds the monovariant peritectic L + Pd_3Si → γ is completely suppressed. The interdendritic liquid becomes enriched in Cu until the monovariant eutectic trough L → γ + κ is encountered. This eutectic completes solidification with no ternary eutectic. On the other hand, the 9 at.% Cu alloy is devoid of dendritic phases and consists of a eutectic of γ and κ. The 12 at.% Cu alloy consists of dendrites of α phase and eutectic of γ and κ. These observations are consistent with the liquidus surface recently proposed by Massalski et al. (5). The point P in Fig. 2b has been moved to agree with the present data. Interestingly the dendritic cores of the α phase contained more Cu than that in the eutectic ($Pd_{55}Cu_{36}Si_8$ compared to $Pd_{73}Cu_{15}Si_{12}$ respectively) indicating a broad stoichiometry for this phase. Additional confirmation that these alloys complete crystallization with the same

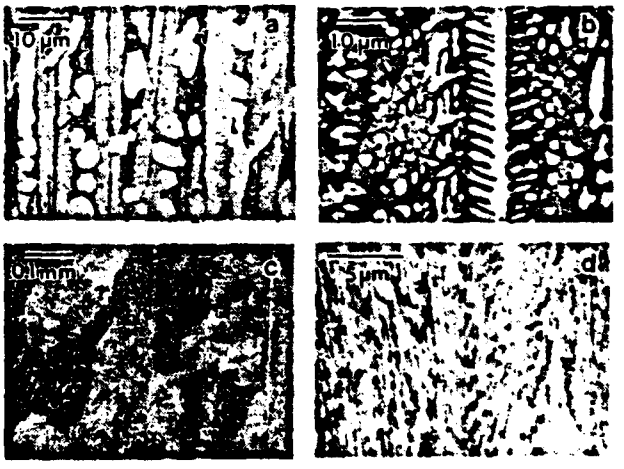

Fig. 3. Structure of 4 at.% Cu alloy at a) 0.25 mm/s, b) and c) 5 mm/s d) 10 mm/s. Growth direction vertical.

eutectic was provided by cooling curves which all showed a final eutectic arrest at 734 2°C.

For alloys with 6 at.% Cu or less, the following changes in microstructure occur at increasing velocities specified in Fig. 2a. a) The dendrites of , phase disappear while the dendrites of Pd_3Si remain and the volume fraction of eutectic increases (Fig. 3b). The adjustment is made presumably by a change in volume fraction of the , phase in the eutectic, necessitating growth of a eutectic-like structure at off-eutectic compositions. b) The dendritic phase of Pd_3Si disappears leaving a structure fully composed of eutectic material (Fig. 3d). c) The eutectic structure, often of a complex morphology, becomes more refined until a sharp interface is formed during the acceleration mode which separates the eutectic from glassy alloy (Fig. 4a,b). The glass occupies the remaining length of the sample. The elimination of the dendritic structure and conversion of the microstructure to fine eutectic is a necessary precursor of glass formation. Also it should be noted that for the 1.4 and 4 at.% Cu alloys, a completely eutectic structure is not observed at steady state, nor are the eutectic grains (colonies) continuous in the growth direction at speeds greater than 2.5 mm/s (Fig. 3c).

The 9 at.% Cu alloy behaves quite differently. The eutectic microstructure becomes more refined with increasing velocity until at 2.5 mm/s, the structure converts to a mixture of glass alloy and 25 µm diameter crystallites (Fig. 4c). A facetted eutectic interface forms which separates the regions. The crystallite size is constant in the remaining length (5 cm) of the sample. Quenching at higher rates of up to 1 cm/s still leads to a mixture of crystallites and glass. The crystallites, when observed by TEM, are dendritic with amorphous interdendritic regions. The dendrites appear to have high Cu content and are presumably · phase. Further confirmation of this is necessary. The 12 at.% Cu alloy also contains these crystallites

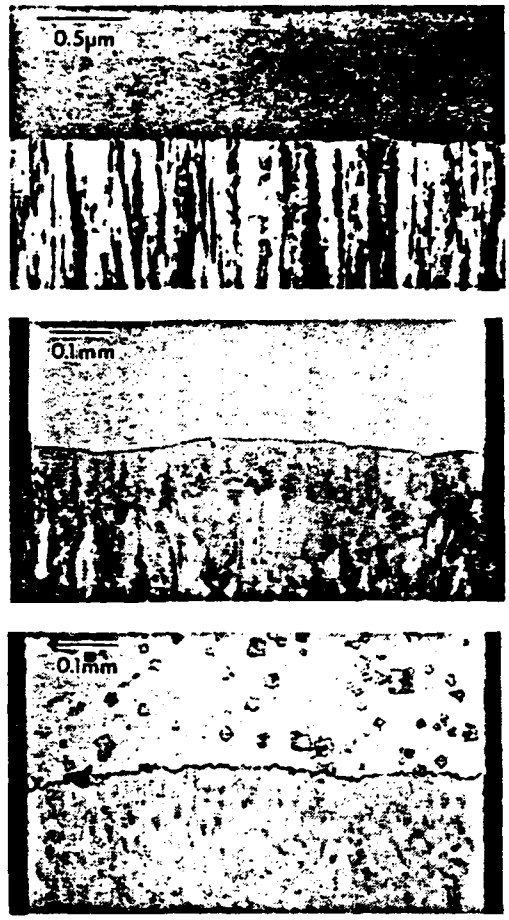

Fig. 4. Interface between eutectic and glass in a) 6 at.% Cu, TEM, b) 4 at.% Cu and c) 9 at.% Cu. Growth direction vertical.

at a quenching speed of 10 mm/s. Their formation directly from the melt even in the presence of a crystalline substrate indicates the importance of nucleation on the high Cu side of the eutectic trough.

DISCUSSION

The maximum growth rate for the eutectic in these experiments is 2.5 mm/s as seen for the 6 at.% Cu alloy. For lower Cu contents the increase in the critical velocity to form glass with decreasing Cu content (Fig. 2a) is related to the velocity required to eliminate dendritic solidification as described in the Introduction. At growth velocities greater than 2.5 mm/s for the 1.4 and 4 at.% Cu alloys, the continuous directional growth of dendrites of Pd_3Si provides nucleation sites for the

eutectic grains which can subsequently grow laterally at much slower speeds to complete crystallization. Evidence for this is found in the lack of continuity of eutectic grains in the growth direction at quenching speeds greater than 2.5 mm/s. For these alloys, this lateral growth of the eutectic prevents the observation of the dendrite + glass microstructures described previously. Once the dendrites have disappeared from the microstructure, the eutectic structure would be required to grow in a continuous directional manner at speeds beyond its maximum. This is impossible and causes the extremely short length of the eutectic structure during acceleration of the growth velocity and the subsequent formation of the sharp interface separating the eutectic structure from the amorphous alloy.

The 9 at.% Cu alloy contains no primary phases at slow cooling rates. It is therefore close to the monovariant eutectic and yet does not form entirely glassy structures at 2.5 mm/s. It is not the easiest glass former. Although the eutectic structure does exhibit a maximum crystallization rate close to 2.5 mm/s, the conversion to a completely glasssy structure is prevented by the formation of dendritic crystallites which nucleate directly from the liquid. Because of this nucleation, the growth analysis presented in the Introduction does not apply on the high Cu side of the eutectic trough. The existence of glass + crystal structures at intermediate cooling rates for these compositions has been previously reported (6). However, the fact that the crystallites form even in the proximity to a substrate yields further information about their formation. The rapid growth of the eutectic at speeds near its maximum requires substantial interface undercooling to temperatures of the order of T_g. The liquid ahead of the growth front must itself be undercooled some distance ahead of the interface. This apparently permits the nucleation and partial growth of the crystallites. The initial growth of these crystals may be assisted by the proximity of these high copper alloys in the undercooled state to the T_o surface for the ϵ phase. Although the position of this surface is unknown, the large range of stoichiometry for copper observed for this phase suggests that its free energy curve is quite broad and its T_o surface extends substantially toward the monovariant eutectic. Below a T_o surface, partitionless crystallization (no solute rejection) is possible and should have extremely fast kinetics. For alloys low in copper, the T_o surfaces for the silicides should extend only slightly into the ternary due to the limited solubility of copper in them. This prevents the formation of isolated silicide crystallites in that composition range and permits the growth model presented to apply.

ACKNOWLEDGMENTS

The author would like to thank F. S. Biancaniello, C. E. Brady, D. E. Newbury, G. M. Kalonji and L. K. Ives.

REFERENCES

1. W. J. Boettinger, F. S. Biancaniello, G. M. Kalonji and J. W. Cahn, in Rapid Solidification Processing II, Claitor's, Baton Rouge (1980) p. 50.
2. K. A. Jackson, Trans. Met. Soc. AIME, 242 (1968) 1275.
3. H. E. Cline and J. D. Livingston, Trans. Met. Soc. AIME, 245 (1969) 1987.
4. E. Scheil and Y. Masuda, Aluminum, 31 (1955) 51.
5. T. B. Massalski, Y. Kim, L. F. Vassamillet and R. W. Hopper, Mat. Sci. and Engineering, 47 (1981) P1.
6. M. Naka, Y. Nishi and T. Masumoto, in Rapidly Quenched Metals III, Vol. 1, Metals Society, London (1978) 231.

O BE PUBLISHED, Rapidly Solidified Amorphous & Crystalline Alloys, ed. by B. H. Kear and B. C. Giessen, Elsevier North Holland, New York 1982.

GROWTH KINETIC LIMITATIONS DURING RAPID SOLIDIFICATION

William J. Boettinger
Metallurgy Division, National Bureau of Standards, Washington, DC 20234, USA

ABSTRACT

The importance of growth kinetics in the development of the microstructure of rapidly solidified alloys is described. Growth kinetics are conveniently divided into diffusion kinetics and interface attachment kinetics. The former, which are used extensively for the analysis of slow rate solidification, can be extended to high solidification rates to predict some microstructural features; e.g., the limitations on eutectic growth rate which can promote the formation of metallic glass, and the reduction of microsegregation. At the highest rates interface attachment kinetics must be included. Some microstructural effects of the velocity dependence of the partition coefficient will be described.

INTRODUCTION

The details of the nucleation and growth kinetics of solid phases from the liquid state generate the wide variety of microstructures observed in cast materials. Nucleation has a dual role: it provides the initial phase selection among the various possibilities and also, when significant undercooling is achieved prior to nucleation, it provides a supercooled liquid into which crystal growth can occur rapidly. Given the wide temperature spectrum of catalytically potent nucleation sites that exists in alloys [1], and the differences in the growth rates of the phases observed, microstructures may in many cases be the results of the competition of various forms of crystal growth. A simple example is found in the columnar zone of a casting where a strong preferred grain orientation is developed even though the chill zone contains a random distribution of grain orientations. The focus of this paper is to describe some growth kinetic limitations that exist for different types of crystallization from the liquid. These limitations can have a strong influence on the microstructure of rapidly quenched alloys. In all cases we will assume that the phases present, whether stable or metastable, have been previously specified. In the present paper the term growth kinetics will be used in its broadest sense; i.e., it will include heat flow, diffusion, and interface attachment kinetics.

INTERFACE CONDITIONS

The analysis of the growth of a single crystalline phase into a two component liquid requires the solution of a complex moving boundary problem. In the absence of fluid flow, diffusion equations for solute and heat must be solved in the liquid and solid phases subject to conservation equations at the liquid-solid interface and a pair of response functions [2]. Of the various choices for dependent and independent variables in these functions, a convenient pair establishes the interface temperature, T_I, and the solid composition at the interface, C_S^*, as functions of the liquid composition at the interface,

C_L^*, the interface mean curvature, K, and the normal interface velocity, v. In their general form, the response functions can include many other variables such as crystal orientation, defect density and absolute temperature which will be neglected here. The response functions can be written as:

$$T_I = T_M - mC_L^* - T_M\Gamma K - f(v,C_L^*) \tag{1}$$

$$C_S^* = k_E C_L^* g(v,C_L^*). \tag{2}$$

The expression $T_m - mC_L^*$ represents the liquidus curve of the alloy (here taken as a straight line with a pure solvent melting point of T_m and slope of m). The term $T_m\Gamma K$ is the depression of the melting point due to interface curvature with Γ the capillarity constant which is usually given as the ratio of the liquid-solid surface tension to the latent heat per unit volume of solid. The parameter k_E is the equilibrium partition coefficient, which in principal also depends on curvature [3]. This curvature effect will be neglected here. The functions f (kinetic undercooling) and g describe the deviations from local equilibrium due to interface attachment kinetics. These functions should have the properties that

$$f(0,C_L^*) = 0 \tag{3}$$

$$g(0,C_L^*) = 1 \tag{4}$$

The expression $k_E g(v,C_L^*)$ is the velocity dependent partition coefficient which, it is reasonable to assume, should approach unity at high velocity. The term, solute trapping, refers to the case when the partition coefficient deviates from the equilibrium value and tends toward unity. The term, complete trapping or partitionless solidification, refers to the case when the partition coefficient is unity. The changing partition coefficient is extremely interesting and important because it can leave behind in the material a changed pattern of microsegregation.

The possible forms for the functions f and g are further constrained by thermodynamics [2]. Implicit in this constraint is the assumption that while local equilibrium across a liquid-solid interface can be lost, the free energies of individual phases are still given at a point by the composition and temperature at that point. This assumption will be adopted here. The constraint is derived using the tangent intercept method applied to free energy-composition curves for the liquid and solid phases. An alternate presentation of this constraint is given in Figure 1, which shows the range of possible solid compositions which can form on solidification at various interface temperatures for a fixed liquid composition at a flat interface. For a curved interface, the phase diagram and range of compositions is depressed in temperature by an amount $T_m\Gamma K$. When the interface is at the liquidus temperature for the liquid composition at the interface only solid of one composition can form. With increased kinetic undercooling a range of compositions of solids can form. Of particular interest is the T_o curve (shown dashed) which lies between the liquidus and solidus. The T_o curve is the locus of compositions and temperatures where the liquid and solid free energies have the same value.

It represents the highest interface temperature at which the partition coefficient can be unity. Generally, further kinetic undercooling should be required for partitionless solidification. One important consideration is that partitionless solidification is impossible for some alloy compositions when the T_o curve falls rapidly to extremely low temperatures (Fig. 1b). In practice then, the limit of the partition coefficient at high velocity cannot approach unity for these compositions. Such a limit on solute trapping is one reason for retaining the C_L^* dependence in f and g.

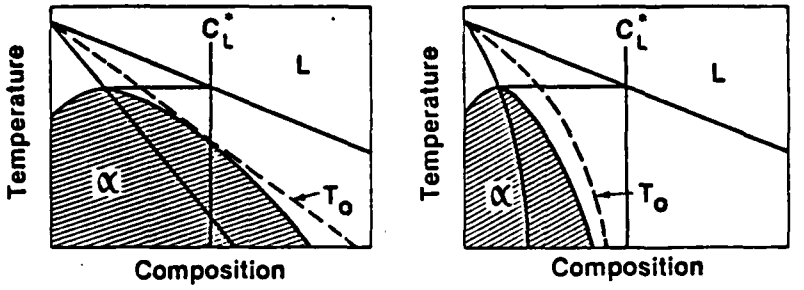

Fig. 1. The shaded region is the range of possible solid compositions, C_s^*, which can form from liquid composition at the interface, C_L^*, at various interface temperatures. Partitionless solification is possible in (a) and impossible in (b).

Various forms for the kinetic undercooling function have been investigated [4-6]. For the non-facetted growth of metals at moderate growth rates, the function f can be taken as linear in the growth rate. Typically, growth at 1 cm/s is expected to require a kinetic undercooling of the order of 0.1 to 1 K. The experimental observation [7-9] of the degree of the velocity dependence of the partition coefficient has generated recent theoretical investigation [10-14]. In laser melted Si doped with Bi, a growth rate of the order of 3 m/s is required to cause a change in the partition coefficient from the equilibrium value of 4×10^{-7} to 0.25. A simple model of solute trapping to envision [12], permits solute to be incorporated into the solid with the same composition as the liquid at the interface. Diffusion of solute back into the liquid attempts to establish the equilibrium solid composition. This process is however halted by the formation of the next layer of crystal. As such, many of the theories [10-12,14] predict that the function $g(v,C_L)$ is an exponential function of a parameter, $v\ell/D$, where D is a diffusion coefficient and ℓ is a distance typically between one and one hundred times the interatomic dimensions. The theories differ in the form of the function and the length and diffusion coefficient employed. As pointed out by Aziz [12] the exponential dependence indicates that the change from equilibrium partitioning to the maximum level of solute trapping will most likely occur over an order of magnitude increase in growth rate. Such a sharp transition may support arguments

[15] that complete trapping occurs during the rapid growth rates following nucleation, but equilibrium partitioning occurs immediately after recalescence in some rapidly solidified alloys.

Cautions in the use of this approach to the interface conditions are abundant. As already mentioned orientation and defect density can be very important. The so-called "facet effect" observed in Czochralski growth of semiconductor compounds [16] where the partition coefficient depends on the crystallographic orientation of the liquid-solid interface is a case in point. The effect of interface curvature on the melting point is also bothersome. In addition to the usual difficulties involving the surfaces of solids [17], deviations from equilibrium, specifically the fact that $C_S^* \rightarrow C_L^*$, certainly will change the value of the surface tension employed.

Although it seems widely accepted that rapid solidification is a non-equilibrium process, it is interesting to note that quite a few microstructural trends as the solidification velocity increases can be predicted by a careful examination of the effects of heat and solute diffusion and interface curvature without requiring the inclusion of interface attachment kinetics into the analysis. In the case of dendritic growth of a pure material into an undercooled liquid, Glicksman, Schaefer, and Ayers [18] and Huang and Glicksman [19] have seen excellent agreement between theory and experiment for dendrite tip speeds up to 1.5 cm/s without including the effects of attachment kinetics. The growth is determined by diffusion of heat and tip curvature. Other microstructural trends clearly require the inclusion of attachment kinetics; e.g., extended solubility of a phase with a retrograde solidus. The relative importance of interface attachment kinetics and diffusion kinetics remains an active area of theoretical and experimental research.

HEAT FLOW

The most widely used parameter to describe rapidly solidified microstructure is the cooling rate. As seen in Eqs. (1) and (2), the interfacial growth velocity and undercooling are of more fundamental importance in growth theories. These parameters and the associated liquid and solid temperature gradients bear a complex relation to the cooling rate of the rapid quenching device employed as well as the degree of undercooling achieved in the liquid before growth is initiated. It is of interest here to estimate the maximum solidification velocities which can be expected in varous rapid quenching geometries. The estimates will be made for the plane front growth of pure metals with zero kinetic undercooling.

In substrate quenching when little undercooling occurs before growth is initiated, the maximum solidification rate is determined by the heat transfer coefficient, h, between the substrate and the alloy melt. The heat transfer coefficient is rarely believed to exceed 10 W/cm^2K [20,21]. Mehrabian [20] has shown that for Biot numbers ($\frac{hl}{k}$) less than 10^{-2}, cooling can be considered Newtonian and then

$$v = \frac{h\Delta T_\infty}{\Delta H} \quad . \tag{5}$$

The parameter l is the melt thickness, k is the alloy thermal conductivity, ΔT_∞ is the difference between the melt temperature and substrate temperature

and ΔH is the latent heat per unit volume. For typical values of these parameters for Al the Biot number is less than 10^{-2} for melt thickness up to 100 μm and the maximum attainable velocity is of the order of 10 cm/s. The temperature gradient in the liquid is positive in this case. When significant undercooling of the liquid occurs, the latent heat can flow into both the liquid and solid and the growth rates can be significantly higher.

In surface melting, intimate contact is maintained between melt and substrate and the growth velocity is controlled by the conduction of heat into the solid. For one-dimensional heat flow and with a heat flux applied for a time just sufficient for the melt surface to reach the temperature where the vapor pressure of the metal is 1 atm, the solidification rate after melting to various depths is relatively uniform over 80 percent of the melt thickness and is given in Table 1 for Al [22]. In this case also the temperature gradient in the liquid should be positive.

TABLE I
Surface melting of Al [22]

Heat Flux W/cm^2	Melt Depth μm	Solidification Velocity cm/s
3×10^7	1	2000
3×10^6	10	200
3×10^5	100	20

In atomization it is difficult to estimate the achievable growth rates simply. As with the case of substrate quenching, the solidification rate is determined by the heat transfer coefficient for the radiative or convective cooling if little undercooling is achieved before growth is initiated. Such coefficients are typically an order of magnitude smaller than those occurring in substrate quenching [20]. When significant undercooling is achieved, the growth rate during recalescence depends on the degree of undercooling and the interface attachment kinetics [23,24]. The growth rate is strongly time dependent and effectively independent of external cooling [23]. Only in the cases where the undercooling exceeds the ratio of the latent heat/unit volume to the liquid heat capacity/unit volume, can the entire sample solidify without recalescence to the melting point and a concomittant reduction of the growth velocity to a value determined by the external heat extraction rate. Because of the time dependence of the growth rate and because of complications of growth when the liquid temperature gradient is negative (which will become apparent), the discussions presented in this paper will generally apply to growth controlled by the heat extraction rate into the solid.

DIFFUSION KINETICS AND INTERFACE CURVATURE

Eutectic growth

Neglecting interface attachment kinetics and including the effects of interface curvature, the analysis of the diffusion of solute in the liquid ahead of a freezing interface yields several kinetic models. A particularly simple kinetic relation exists for the growth of a rod or lamellar eutectic structure [25]. The analysis is simple because the eutectic grows with a relatively flat liquid-solid interface and the temperature gradient is not important. The governing equation for the difference between the eutectic temperature, T_E, and the interface temperature can be given in terms of the growth velocity, V, and the eutectic spacing, λ, as

$$T_E - T_I = \Delta T = \frac{A_1}{D_L(T_I)} \lambda V + \frac{A_2}{\lambda} \tag{6}$$

The parameters A_1 and A_2 are $\bar{m}\Delta C/8$ and $2\gamma_{\alpha\beta}/\Delta S$ respectively, where $\bar{m}$ is an average positive liquidus slope of the two phases, ΔC is the composition difference between the two solid phases, $\gamma_{\alpha\beta}$ is the surface energy between the solid phases, ΔS is an average entropy of fusion of the solid phases and D_L is the liquid interdiffusion coefficient. Equation (6) shows directly the requirements for the diffusional sorting of the components into the two solid phases (first term RHS) and the presence of curved lamellar growth fronts to satisfy the trijunction with the solid-solid surfaces (second term RHS). The equation permits a range of velocities for a given interface temperature depending on the spacing. The maximum rate at which the eutectic structure can grow at a given interface temperature is given by

$$V = \frac{D_L(T_I)(\Delta T)^2}{4A_1A_2} \quad , \tag{7}$$

and the eutectic spacing is given by

$$\lambda = 2A_2/\Delta T \quad , \tag{8}$$

or

$$\lambda^2 V = D_L(T_I)A_2/A_1 \quad . \tag{9}$$

The inclusion of the temperature dependence of the liquid interdiffusion coefficient with Arrhenius behavior with even a modest activation energy leads to maximum growth rate for eutectics of about 10 cm/s at an undercooling of the order of 100 K below the eutectic temperature. Extensive measurements have been made for Pb-Sn at growth rates up to 1 mm/s [26,27]. Taking this data to determine the constants A_1 and A_2 with $D_L = 6\times10^{-6}$ cm^2/s [28] near the eutectic temperature, the growth rate at various interface temperatures can be calculated. A plot of Eq. (7) is shown in Figure 2 using an activation energy of 5 kcal/mole K to extend the diffusion coefficient to large undercoolings. This maximum growth rate is smaller than the growth rate required by the heat extraction rate which occurs in many rapid quenching techniques and presents a real growth rate limitation.

The maximum velocity for eutectic growth can be reduced by an order of magnitude by other effects. First, if one of the phases in the eutectic has high entropy of fusion (> 2R) it may exhibit growth facets and have difficulty in branching in order to reduce its eutectic spacing to the value required for optimum growth rate. The effect has been described in detail by Fisher and Kurz [29]. This effect generally leads to larger eutectic spacings for a given velocity than is observed for non-facetted eutectics (i.e., a larger $\lambda^2 V$ constant) and a larger undercooling for a given velocity. A second effect is found if the diffusion coefficient exhibits a large decrease due to the proximity of a glass transition in the liquid phase.

For high speed eutectic growth the positions of the metastable solidus curves and the velocity dependence of the partition coefficients for the two solid phases may become important. This would be reflected in a reduction of ΔC, the difference in composition between the two solid phases. The latter effect will depend critically on the positions of the T_o curves in the phase diagram. These curves determine a thermodynamic bound on the solid phase compositions which can form. Figure 3 shows three possibilities for the T_o curves in simple eutectic systems. In Figure 3a, very little extension of

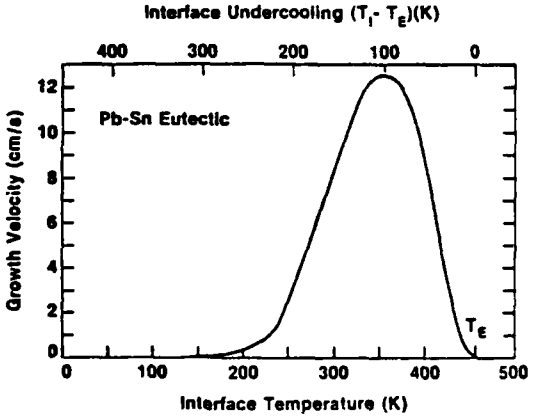

Fig. 2. The calculated rate of growth of the Pb-Sn eutectic as a function of interface temperature extrapolated from low velocity experimental results [26,27] using an activation energy of 5 kcal/mole. The maximum growth rate is 12.5 cm/s.

solubility is possible and the maximum growth rate of the eutectic would be unaffected. Alloys undergoing eutectic growth in this type of system should be strong candidates for glass formation [30]. In alloys such as shown in Figure 3b and c, the reduction of ΔC may permit eutectic growth at higher rates than in the case of Figure 3a, but more importantly the undercooling required to drive the eutectic interface at high rate can approach that required for partitionless solidification of one or both of the phases. (In the case of Figure 3c, the two phases are the same but separated by a miscibility gap.)

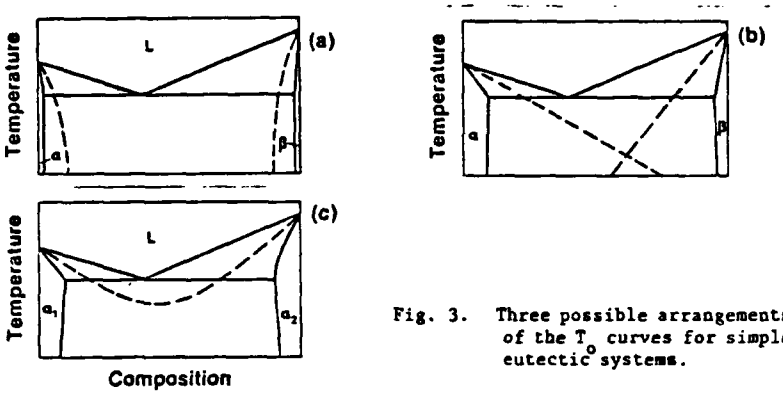

Fig. 3. Three possible arrangements of the T_o curves for simple eutectic systems.

Examples of the limits of eutectic growth at high speed can be found in Pd-Cu-Si and Ag-Cu alloys. The Pd-6at.% Cu-17at.% Si easy glass forming alloy contains a binary eutectic between an orthorhombic phase Pd_9Si_2, and a cubic phase, κ, rich in copper [30,31]*. At slow rates this alloy consists of dendrites of Pd_9Si_2 and Pd_3Si and eutectic, but at higher rates (~ 1 mm/s) becomes devoid of these dendrites and solidifies as a binary rod type eutectic structure. The phases have different crystal structures and appear to have a ternary analogue of the type of phase diagram shown in Figure 3a. Ag-Cu of course has a phase diagram of the type shown in Figure 3c. Using a directional quenching furnace which can provide for controlled growth at speeds up to about 5 cm/s, the Pd-Cu-Si alloy was shown to have a maximum growth rate of 2.5 mm/s. At attempted growth beyond this speed, metallic glass was formed. Figure 4 shows a bright field electron micrograph of the sharp interface found between the crystalline material and amorphous alloy. It is believed that the vicinity of this interface represents the position in the sample where the isotherm velocity exceeded the maximum growth rate of this eutectic. The low maximum velocity of this eutectic is clearly assisted by the well known high T_g of the alloy, but also by the facetted nature of one of the phases in the eutectic. The Ag-Cu eutectic, when splat cooled, solidifies into a single supersaturated F.C.C. phase [32,33]†. Because the metastable solidus curves are retrograde [34], the solidification most likely is partitionless. Figure 5 shows a columnar single phase structure obtained by melt spinning. Directional quenching experiments of this alloy at speeds up to 2.5 cm/s have failed to produce this microstructure. Laser surface melting [35] has however succeeded in producing the single phase. Clearly it is of great interest to determine the growth speeds at which the transition from eutectic growth to single phase growth occurs. In the case of Ag-Cu, the T_o curve is only about 100 °C below the eutectic temperature. It appears likely that in this case eutectic growth will be replaced by partitionless solidification at growth velocities where the eutectic interface temperature falls below the T_o curve for the alloy.

* κ-phase has an approximate composition of $Pd_{73}Cu_{15}Si_{12}$ is cubic and does not exhibit growth facets. Pd_9Si_2 is facetted.

† Supersaturated solid solutions obtained in this system can lie within a spinodal and can quickly decompose in the solid state [33].

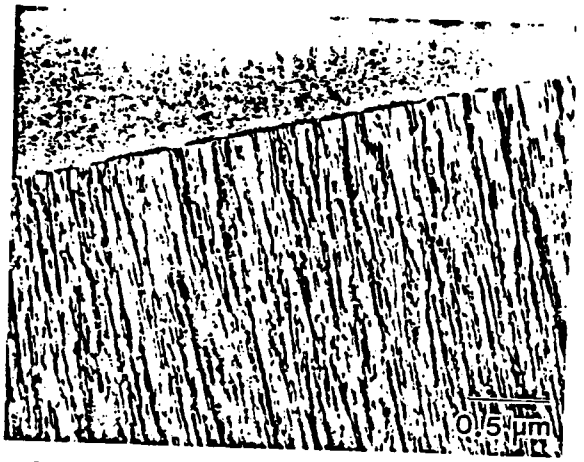

Fig. 4. Interface between fine eutectic structure and amorphous alloy obtained in a Pd-6 at.% Cu-17 at.% Si alloy when growth was attempted at 2.5 mm/s. TEM.

Fig. 5. Columnar single phase structure obtained in melt spun Ag-Cu eutectic alloy. Wheel side is at the bottom.

The Coupled Zone

The range of alloy compositions which undergoes eutectic solidification without primary phases at a given growth rate may or may not include the thermodynamic eutectic composition. Frequently the range of compositions, referred to as the coupled zone, expands and shifts in composition as the growth

rate (or interface undercooling) is increased. Originally [36-38] coupled zones were determined as a function of melt undercooling prior to nucleation. Kobayashi and Shingu [39] have measured the growth rates of eutectic and dendritic structures in Pb-Sn undercooled alloys. Other work, performed with the directional solidification technique up to growth velocities of ~ 0.5 cm/s, has been reviewed by Kurz and Fisher [40]. This technique permits the measurement of the interface temperature and control of the velocity for coupled growth. Two types of coupled zones are shown in Figure 6. The boundaries of the coupled zone at slow velocities (< 10^{-3} cm/s) or small undercoolings are

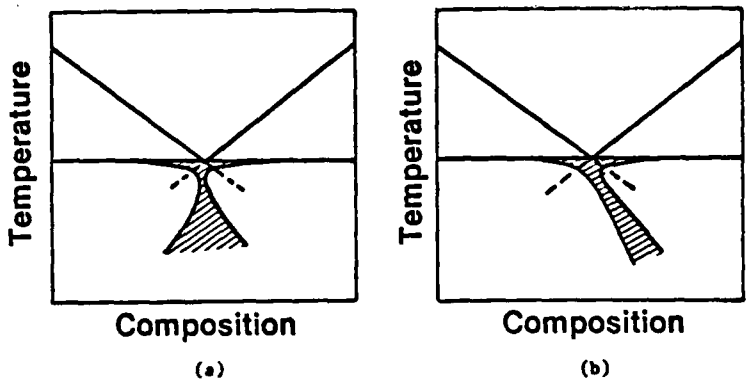

Fig. 6. (a) Symmetric and (b) asymmetric coupled zones showing interface temperatures and composition where coupled eutectic growth occurs. In (b) the phase on the right is facetted.

strong functions of the liquid temperature gradient and correspond roughly to a constitutional supercooling criterion [41]. This part of the coupled zone can be extremely wide and is used for the growth of off-eutectic composite structures. The higher velocity regime is of more interest in the present paper because it determines a limitation on the range of velocity and compositions where dendritic and eutectic structures are observed.

The symmetric coupled zone shown in Figure 6a is typical of eutectics involving two non-facetted phases; e.g., Ag-Cu, Pb-Sn. The asymmetric coupled zone in Figure 6b is typical of a eutectic between a non-facetted and a facetted phase; e.g., Al-Al_6Fe, Ni-Ni_3Nb. In the latter case, the coupled zone shifts toward the facetted phase as the growth rate is increased. It is interesting to note that systems with symmetric coupled zones have relatively symmetric T_o curves while alloys with asymmetric coupled zones have asymmetric T_o curves*. The coupled zone shifts away from the phase with the larger potential for solubility enhancement. This fact may be significant for the continued shifting of the coupled zone at higher growth rates.

* The T_o curve for an intermetallic compound of limited range of stochiometry does not extend very far compositionally from the compound due to the narrow range of the free energy curve for the compound.

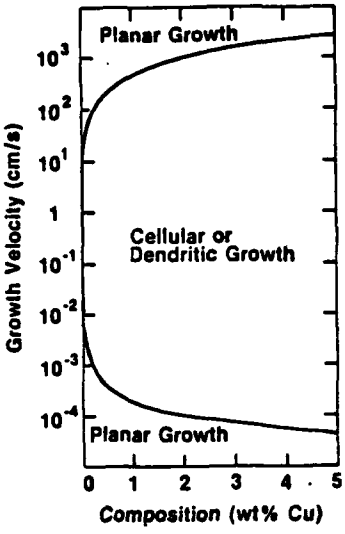

Fig. 7. Calculated growth velocity for various Al-Cu alloys delineating the range of stability of planar growth. The liquid temperature gradient was taken as 100 K/cm.

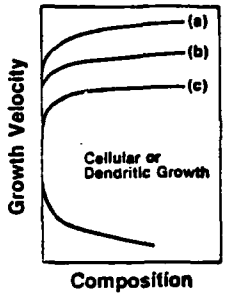

Fig. 8. The effect of the velocity dependence of the partition coefficient on the limit of stability for planar growth (a) is shown schematically for increasing levels (b), (c) of solute trapping.

solute segregation as a function of growth rate for a fixed interface shape and show changing microsegregation curves. Clearly this area long with the secondary dendrite arm coarsening problem remains ripe for investigation.

SUMMARY

In this paper various limitations on dendritic and eutectic growth have been described. Figure 9 summarizes schematically the microstructures which may be observed for various compositions and growth rates for the three phase diagram types shown in Figure 3. Such diagrams represent the extremes of simplification and may only apply when the temperature gradient in the liquid is positive. These diagrams are also drawn with the realization that the temperature gradient is very important at slow growth rates but is of less importance at high growth rate. This fact is reflected in the theories of the boundaries of both the coupled zone and the regime of absolute stability. Figure 9a shows the case for a system like Ag-Cu, where the T_o curve is only about 100 °C below the stable liquidus. The regions on the extreme right and left and connected at high growth rate represent microstructures consisting of a single crystalline phase free of microsegregation. The boundary between this region and the regions where dendritic growth occurs is given at low

The theory of the boundaries of the coupled zone has been approached in two ways. The first has applied a Mullins and Sekerka type stability analysis to the "planar" eutectic interface [42-45]. Because of the complexity of the unperturbed state, such analysis is extremely difficult. A second approach [46-47], often called a competitive growth theory, calculates the dendritic tip temperature for a given dendritic tip growth rate as a function of alloy composition. This tip temperature is compared to the interface temperature of a fully eutectic structure at the same growth rate*. The structure with the highest interface temperature is the predicted morphology. This approach seems to be valid as long as the liquid temperature gradient is positive (heat flows into the solid). Burden and Hunt have solved an approximate solute diffusion problem for the dendrite tip and calculated the dendrite tip temperatures [48] and zone boundaries [49] using the assumption of local equilibrium and employing the extremum principle for the dendrite and eutectic theories. Such an analysis generally predicts symmetric coupled zones. Kurz and Fisher [50] have extended this type of analysis to include a more modern (Langer and Müller-Krumbhaar) replacement of the extremum principle and the effects of the branching difficulties of facetted-nonfacetted eutectics mentioned above. The experimentally observed asymmetry of coupled zones for these eutectics is then obtained.

The importance of an asymmetric coupled zone and the competition between a stable and metastable eutectic in determining the structure of alloys is shown strikingly in the results of Adam and Hogan [51] or Hughes and Jones [52]. For example, hypereutectic Al-4 wt.% Fe alloys at growth rates less than 0.1 mm/s consists of Al_3Fe primary crystals and Al-Al_3Fe eutectic. Between 0.1 mm/s and 0.8 mm/s the alloy consists of Al_3Fe primary crystals and Al-Al_6Fe eutectic. Between 0.8 mm/s and 7 mm/s the alloy is Al-Al_6Fe eutectic. Above 7 mm/s the alloy is primary α-Al and Al-Al_6Fe eutectic. At the highest rates of solidification, these alloys are known to consist entirely of supersaturated α-(Al, Fe) [53].

In another example [31], the easy glass forming composition Pd-17at.% Si-6at.% Cu consists of dendrites of Pd_3Si and Pd_9Si_2 and Pd_9Si_2-κ eutectic at growth speeds below 1 mm/s. At speeds above 1 mm/s the alloy consists entirely of Pd_9Si_2-κ eutectic and as mentioned above forms metallic glass at speeds above 2.5 mm/s. (See Figure 4) In this case the coupled zone is shifting towards the facetted phase Pd_9Si_2 with increasing growth rate. Such shifts may be important in fine tuning the composition near a eutectic which forms metallic glass most easily.

Dendritic Growth

Whereas the boundaries of the coupled zone provide a limit on the conditions of dendritic growth for alloys with large solute content, a different growth limitation can occur for more dilute alloys. For growth into a positive gradient,† there exists a velocity beyond which the plane front growth of

* The eutectic growth rate is only weakly dependent on composition.

† More correctly if $k_s G_s + k_L G_L \geq 0$ where k_s and k_L are the solid and liquid thermal conductivities and G_s and G_L are the solid and liquid temperature gradients.

a single phase solid is morphologically stable. This growth regime is referred to as absolute stability [54]. The result of constitutional supercooling theory cannot be extended to high velocity because it neglects the effect of curvature on the melting point. Surface tension stabilizes the plane front at large growth rates. It is important to note that this theoretical limit does not exist for growth into an undercooled melt. Coriell and Sekerka [55] have recently described the effect of a composition dependent equilibrium partition coefficient and the additional stabilizing effect of interface attachment kinetics on the stability theory. However, metastable liquidus and solidus data and detailed kinetic models are required before concrete predictions of the range of stability can be calculated.

Figure 7 shows the calculated range of growth velocity and composition assuming local equilibrium for α-Al containing Cu where plane front growth is stable. As with the coupled zone boundaries, the part of the curve at low velocity is a strong function of temperature gradient whereas the portion at high velocity is not. Simplified asymptotic expressions for stability for the low and high velocity branches where ΔT is the equilibrium freezing range of the alloy of composition C_o are

$$v < \frac{G^* D_L}{\Delta T} = \frac{G^* D_L k_E}{m(1-k_E)C_o} \tag{10}$$

and

$$v > \frac{D_L \Delta T}{k_E T_M \Gamma} = \frac{m D_L (1-k_E) C_o}{k_E^2 T_M \Gamma} \quad , \tag{11}$$

with

$$G^* = \frac{k_L G_L + k_s G_s}{(k_L + k_s)} \quad . \tag{12}$$

At growth rates of 10^3 cm/s, the characteristic diffusion length D_L/v approaches atomic dimensions, where the continuum approach is invalid. The value of k_E has a strong influence on the velocity required for absolute stability however [56]. Generally the inclusion of interface attachment kinetics will lower the predicted velocity required for planar growth at high velocity as shown schematically in Figure 8. The relative importance of the stabilization due to surface tension and due to interface kinetics remains an important question.

As the growth velocity of a dendritic structure approaches that for absolute stability, it is anticipated that the microstructure will change from dendritic to cellular before becoming plane front. Such a transition will undoubtedly cause an alteration in the microsegregation and secondary dendritic arm spacing behavior due to the reduced times for liquid diffusion and coarsening. Allen and Hunt [57] have concluded that, at growth rates of the order of 1 cm/s, the assumption of complete mixing in the interdendritic region will not be valid. This will cause deviations from Scheil behavior and reduce the volume fraction of eutectic or second phases from that seen at slower growth rates. Similarily Coriell et al. [58] have calculated lateral

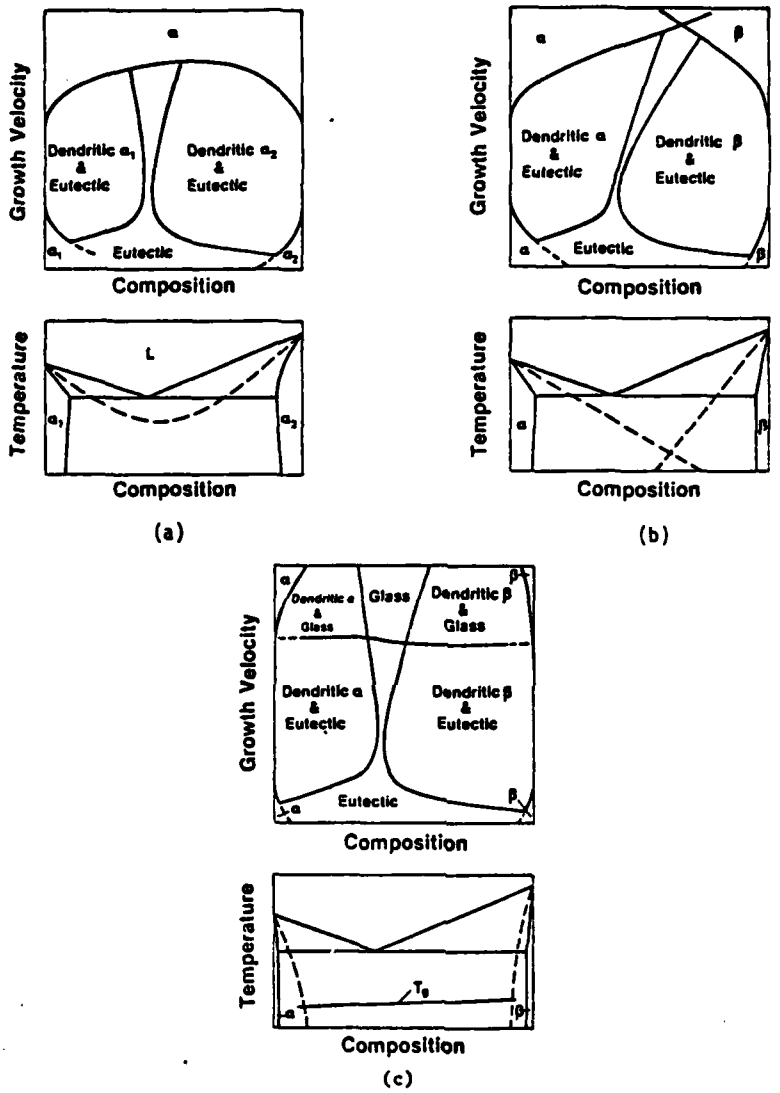

Fig. 9. Schematic growth velocity versus composition plots of the microstructure expected for growth into a positive temperature gradient for simple eutectic systems with (a) a continuous T_o curve, (b) intersecting T_o curves and (c) nonintersecting T_o curves. The symbols α and β refer to single phase structure free of microsegregation.

velocities by constitutional supercooling, at intermediate velocities by absolute stability and at the highest velocities by absolute stability including the velocity dependence of the partition coefficient. The coupled zone for eutectic growth is symmetric and is bounded at high growth rate by partitionless growth of the solid solution. In alloys like Zn-Cd where the T_o curve is depressed by ~ 200 K below the eutectic [34], partitionless growth of the solid solution is not observed at the eutectic composition and some other two phase growth mode may operate [59].

Figure 9b shows the case where the T_o curves for the two phases in the eutectic intersect at a relatively high temperature and where the β phase tends to form growth facets. In this case the coupled zone is asymmetric and is bounded at high velocities by curves for the growth of α or β free of microsegregation. The metastable solidi are most likely not retrograde in this kind of phase diagram. Enhanced solid solubility does not necessarily imply that growth occurred with solute trapping. This diagram may be typical of alloys like Al-Al_6Fe where drastic changes in the growth morphology occur as the growth rate is increased. For example, a single alloy composition can, with increasing velocity, grow as eutectic, dendritic β plus eutectic, eutectic, dendritic α plus eutectic and finally segregation free α.

Figure 9c shows the case of an alloy where very limited solubility extension of the phases in the eutectic is possible. The T_o curves for the two liquid to crystal transformations dive steeply to low temperatures. In such a diagram partitionless solidification is forbidden over a wide range of composition at any growth velocity. The figure shows this case when, in addition, the liquid exhibits a large decrease in diffusion coefficient due to the proximity of a glass transition in the liquid phase. In this case the coupled zone for eutectic growth is bounded by the maximum growth rate for the eutectic into the viscous liquid. Beyond this growth rate metallic glass will form. Dendritic growth with its higher dendrite tip temperatures than eutectic growth at the same speed for compositions outside of the coupled zone will

Fig. 10. Interdendritic amorphous alloy in Pd-9at.% Cu-15at.% Si.

require increasing growth rates as the composition varies away from the coupled zone before completely glassy structures can form. Such is the case for a series of Pd-Cu-Si alloys [31]. In such a system, dendritic growth must be accompanied by solute rejection regardless of growth rate and the interdendritic region will have compositions closer to the coupled zone. For this reason the maximum growth rate curve for the eutectic in Figure 9c is extended into the dendritic and eutectic region. Above this line microstructures of dendrites with interdendritic glass may form. Figure 10 shows a micrograph of such a microstructure in a Pd-Cu-Si alloy. The STEM analysis shows the interdendritic region to have a composition closer to the easy glass forming composition than the average alloy composition. Similarily, an intercellular amorphous phase has been observed to have high phosphorus content in rapidly quenched steels [60].

ACKNOWLEDGMENT

The author is grateful for support of this research to the Defense Advanced Research Projects Agency. Gratitude is expressed to J. W. Cahn, S. R. Coriell, R. Mehrabian, J. H. Perepezko, and R. J. Schaefer for helpful discussions; to G. M. Kalonji and L. K. Ives for electron microscopy; and to F. S. Biancaniello for the solidification experiments.

REFERENCES

1. J. H. Perepezko, in Rapid Solidification Processing: Principles and Technologies II. ed. by R. Mehrabian, B. H. Kear and M. Cohen (Claitor's, Baton Rouge, LA, 1980) 56-67.
2. J. C. Baker and J. W. Cahn, in Solidification (ASM, Metals Park, 1971) 23.
3. M. C. Flemings, Solidification Processing (McGraw Hill, New York, 1974) 273.
4. D. Turnbull, in Thermodynamics in Physical Metallurgy (ASM, Metals Park, 1949).
5. J. W. Cahn, W. B. Hillig and G. W. Sears, Acta Met. 12 (1964) 1421.
6. K. A. Jackson, D. R. Uhlmann and J. D. Hunt, J. Cryst. Growth 1 (1967) 1.
7. K. A. Jackson and M. J. Leamy, in Laser-Solid Interactions and Laser Processing, ed. by M. J. Leamy and J. M. Poate (Am. Inst. of Phys., New York, 1979) 102.
8. R. F. Wood, J. C. Wang, G. E. Gilles and J. R. Kirkpatrick, in Laser and Electron Beam Processing of Materials, ed. by C. W. White and P. S. Peercy (Academic Press, New York, 1980) 37.
9. J. Chikawa and F. Sato, Jap. J. Appl. Physics 19 (1980) L159 and L577.
10. J. C. Baker, Interfacial Partitioning During Solidification, Ph.D. Thesis, MIT (1970) Chapter V. Also reported by J. W. Cahn, S. R. Coriell and W. J. Boettinger, in Laser and Electron Beam Processing of Materials, ed. by C. W. White and P. S. Peercy (Academic Press, NY, 1980) 89-103.
11. K. A. Jackson, G. H. Gilmer and M. J. Leamy, in Laser and Electron Beam Processing of Materials, ed. by C. W. White and P. S. Peercy, (Academic Press, NY, 1980) 104-110.
12. M. J. Aziz, J. Appl. Phys. 53 (1982).
13. M. Hillert and B. Sundman, Acta Met. 25 (1977) 11.
14. R. F. Wood, Appl. Phys. Lett. 37 (1980) 302.
15. M. Cohen, B. H. Kear, and R. Mehrabian, in Rapid Solidification Processing: Principles and Technologies II, ed. by R. Mehrabian, B. H. Kear and M. Cohen (Claitor's, Baton Rouge, LA, 1980) 1-23.
16. W. Bardsley, J. B. Mullin, and D. T. J. Hurle, in Solidification of Metals (Iron and Steel Inst. Publ. #110, London, 1968) 93.
17. J. W. Cahn, in Segregation to Interfaces (ASM, Metals Park, 1978) 3-23.

18. M. E. Glicksman, R. J. Schaefer and J. D. Ayers, Met. Trans. 7A (1976) 1747.
19. S. C. Huang and M. E. Glicksman, Acta Met. 29 (1981) 701.
20. R. Mehrabian, in Rapid Solidification Processing: Principles and Technologies (Claitor's, Baton Rouge, LA, 1978) 9-27.
21. H. Jones, ibid, 28-45.
22. S. C. Hsu, S. Chakravorty and R. Mehrabian, Met. Trans. 9B (1978) 221.
23. C. G. Levi and R. Mehrabian, Met. Trans. 13B (1982).
24. R. J. Schaefer and M. E. Glicksman, J. Cryst. Growth 5 (1969) 44.
25. K. A. Jackson and J. D. Hunt, Trans. TMS-AIME 236 (1966) 1129.
26. R. M. Jordan and J. D. Hunt, Met. Trans. 3 (1972) 1385.
27. H. E. Cline and J. D. Livingston, Trans. TMS-AIME 245 (1969) 1987.
28. J. D. Verhoeven, J. C. Warner and E. D. Gibson, Met. Trans. 3 (1972) 1437.
29. D. J. Fisher and W. Kurz, Acta Met. 28 (1980) 777.
30. W. J. Boettinger, F. S. Biancaniello, G. M. Kalonji and J. W. Cahn, in Rapid Solidification Processing: Principles and Technologies II, ed. by R. Mehrabian, B. H. Kear and M. Cohen (Claitor's, Baton Rouge, LA, 1980) 50-55.
31. W. J. Boettinger, in Rapidly Quenched Metals 4 (Japan Inst. of Metals, Sendai, 1981).
32. R. K. Linde, J. Appl. Phys. 31 (1960) 1136.
33. P. G. Boswell and G. A. Chadwick, J. Mat. Sci. 12 (1977) 1879.
34. J. L. Murray, private communication.
35. D. G. Beck, S. M. Copley, and M. Bass, Met. Trans. 12A (1981) 1687.
36. G. Tamman and A. A. Botschwar, Z. Anorg. Chem. 157 (1926) 27.
37. A. Kofler, Z. Metallkd. 41 (1950) 221.
38. E. Scheil and Y. Musuda, Aluminum 31 (1955) 51.
39. K. Kobayashi and P. H. Shingu, in Rapidly Quenched Metals 4 (Japan Institute of Metals, Sendai, 1981).
40. W. Kurz and D. J. Fisher, Int. Met. Rev. 5-6 (1979) 177.
41. F. R. Mollard and M. C. Flemings, Trans. TMS-AIME, 239 (1967) 1534.
42. H. E. Cline, Trans. TMS-AIME 242 (1968) 1613.
43. R. M. Jordan and J. D. Hunt, J. Cryst. Growth 11 (1971) 141.
44. D. T. J. Hurle and E. Jakeman, ibid. 3/4 (1968) 574.
45. S. Strässler and N. R. Schneider, Phy. Cond. Matter 17 (1974) 153.
46. J. D. Hunt and K. A. Jackson, Trans. TMS-AIME 239 (1967) 864.
47. K. A. Jackson, ibid 242 (1968) 1275.
48. M. H. Burden and J. D. Hunt, J. Cryst. Growth 22 (1974) 109.
49. M. H. Burden and J. D. Hunt, J. Cryst. Growth 22 (1974) 328.
50. W. Kurz and D. J. Fisher, Acta Met. 29 (1981) 11.
51. C. M. Adam and L. M. Hogan, J. Australian Inst. of Met. 17 (1972) 81.
52. I. R. Hughes and H. Jones, J. Mat. Sci. 11 (1976) 1781.
53. H. Jones, Aluminum 54 (1978) 274.
54. W. W. Mullins and R. F. Sekerka, J. Appl. Phys. 35 (1964) 444.
55. S. R. Coriell and R. F. Sekerka, in Rapid Solidification Processing: Principles and Technolgies II, ed. by R. Mehrabian, B. H. Kear and M. Cohen (Claitor's, Baton Rouge, LA, 1980) 35-49.
56. R. J. Schaefer, S. R. Coriell, R. Mehrabian, C. Fenimore, and F. S. Biancaniello, this proceedings.
57. D. J. Allen and J. D. Hunt, Met. Trans. 10A (1979) 1389.
58. S. R. Coriell, R. F. Boivert and R. G. Rehm, J. Cryst. Growth 54 (1981) 167.
59. P. G. Boswell and G. A. Chadwick, J. Mat. Sci. 14 (1979) 1269.
60. T. F. Kelly and J. B. VanderSande, in Rapid Solidification Processing: Principles and Technologies II, ed. by R. Mehrabian, B. H. Kear and M. Cohen (Claitor's, Baton Rouge, LA 1980) 100-111.